UNIVERSITI TEKNIKAL MALAYSIA MELAKA

INVESTIGATION OF STRENGTH MATERIAL FOR ADDITIVE MANUFACTURING USING 3D METAL PRINTER

AHMAD NAZIRUL MUBIN BIN NEZAM
B092010402

BACHELOR OF MECHANICAL ENGINEERING TECHNOLOGY (AUTOMOTIVE TECHNOLOGY) WITH HONOURS

2024

Faculty of Mechanical Engineering Technology

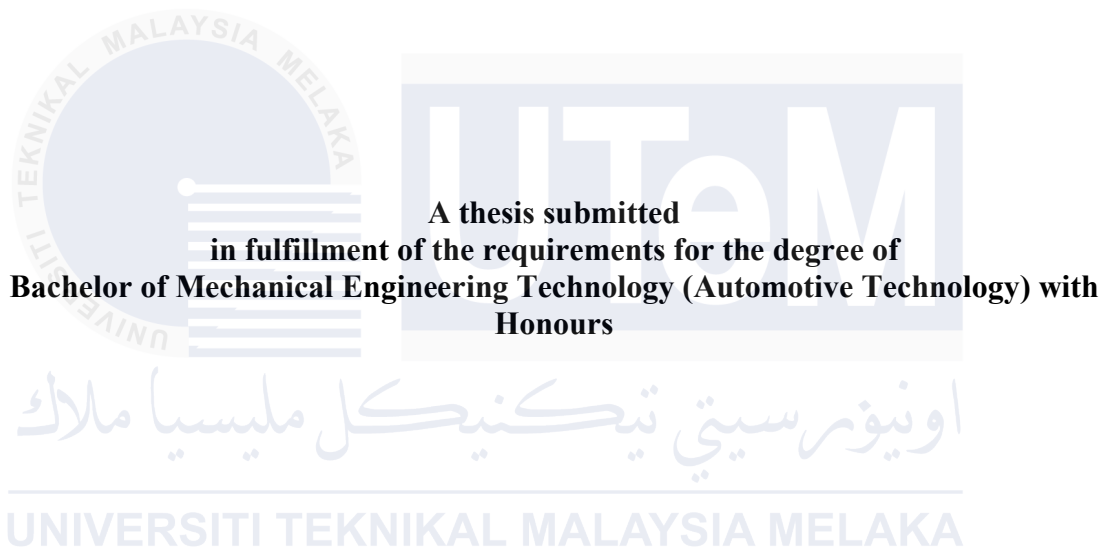**INVESTIGATION OF STRENGTH MATERIAL FOR ADDITIVE MANUFACTURING USING 3D METAL PRINTER**

Ahmad Nazirul Mubin Bin Nezam

Bachelor of Mechanical Engineering Technology (Automotive Technology) with Honours

2024

INVESTIGATION OF STRENGTH MATERIAL FOR ADDITIVE MANUFACTURING USING 3D METAL PRINTER

AHMAD NAZIRUL MUBIN BIN NEZAM

**A thesis submitted
in fulfillment of the requirements for the degree of
Bachelor of Mechanical Engineering Technology (Automotive Technology) with
Honours**

Faculty of Mechanical Engineering Technology

UNIVERSITI TEKNIKAL MALAYSIA MELAKA

2024

DECLARATION

I declare that this Choose an item. entitled "Investigation Of Strength Material For Additive Manufacturing Using 3D Metal Printer" is the result of my own research except as cited in the references. The Choose an item. has not been accepted for any degree and is not concurrently submitted in candidature of any other degree.

Signature	:	
Name	:	Ahmad Nazirul Mubin Bin Nezam
Date	:	10th January 2024

APPROVAL

I hereby declare that I have checked this thesis and in my opinion, this thesis is adequate in terms of scope and quality for the award of the Bachelor of Mechanical Engineering Technology (Automotive Technology) with Honours.

Signature   :

Supervisor Name :   Ts. Dr. Mohd Basri Bin Ali
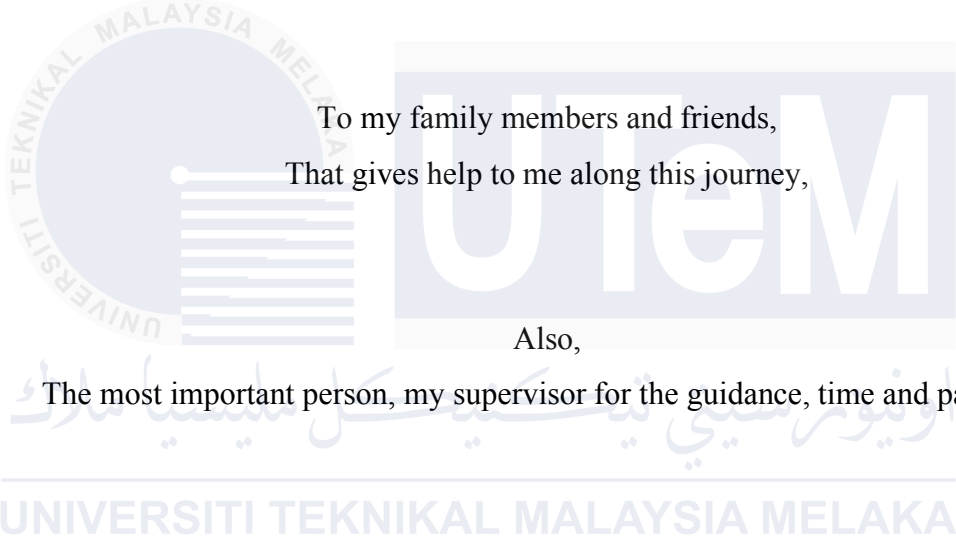
Date   :   10th January 2024

DEDICATION

To my parents and partner,

That gives me unconditional loves and support towards completing this report,

To my family members and friends,

That gives help to me along this journey,

Also,

The most important person, my supervisor for the guidance, time and patience,

And lastly,

For those whoever pray for my success in my life.

ABSTRACT

Additive manufacturing of materials is also known as 3D Printing. 3D Printing is a novel and rapid emerging technology in automotive industry. As the autmotive industry is one of the most competitive industries worldwide, new market and design trends emerge continuously, requiring new manufacturing approaches to comply with the automotive industry.Additive manufacturing provides an important competitive edge to this industrial domain, acting as a disruptive approach by shortening products design and development, delivering flexibility on production and producng optimized automotive components and customized vehile products uopn request. Among the 3D printing techniques, Selective Laser melting (SLM) is one of the effective technique in additive manufacturing process. The main objective of this thesis is to study the strength material for additive manufacturing of S 316L-A11 powder with different specimen thickness and orientations. In this study, specimens were prepared according to ASTM Standard E23 for Charpy impact test and ASTM E8 for tensile test and the same standard was also applied for the laboratory testing respectively. The Charpy specimens were fabricated to different thickness of 5mm, 7.5mm and 10mm by using Ermaksan Enavision 120 SLM 3D Printer. This study parameter selection are 230V, 5m/s scanning speed, 32A, 300W scanning speed, argon and nitrogen as inert gases, and 2500 ppm of oxygen level. Charpy Impact Test on the specimens are performed on the flat samples and subsequent materials comparison are frequently conducted against results obtained from impact tests perfomed using Charpy specimens. The absorbed energy, strain gauge signal and tensile test results the strength material of S 316 L-A11. The result shows that specimen of S 316 L-A11 with thickness of 10.0mm has the greater absorbed energy value. The area under the strain-time graph, maximum strain and absorbed energy are all significantly influenced by thickness of specimens. This study also made a comparison between strain-time graph between S 316 L-A11 and SS304. The result of the comparison shows that S 316 L-A11 is more preferable material to be used in additive manufacturing due to the material strength.

ABSTRAK

Pengilangan bahan tambahan juga dikenali sebagai Percetakan 3D. Percetakan 3D ialah teknologi baru dan pesat muncul dalam industri automotif. Memandangkan industri automotif merupakan salah satu industri yang paling kompetitif di seluruh dunia, trend pasaran dan reka bentuk baharu muncul secara berterusan, memerlukan pendekatan pembuatan baharu untuk mematuhi industri automotif. Pembuatan aditif memberikan kelebihan daya saing yang penting kepada domain perindustrian ini, bertindak sebagai pendekatan yang mengganggu oleh memendekkan reka bentuk dan pembangunan produk, memberikan fleksibiliti pada pengeluaran dan menghasilkan komponen automotif yang dioptimumkan dan produk kenderaan yang disesuaikan dengan permintaan anda. Antara teknik cetakan 3D, Selective Laser melting (SLM) merupakan salah satu teknik yang berkesan dalam proses pembuatan aditif. Objektif utama tesis ini adalah untuk mengkaji bahan kekuatan untuk pembuatan bahan tambahan serbuk S 316L-A11 dengan ketebalan dan orientasi spesimen yang berbeza. Dalam kajian ini, spesimen telah disediakan mengikut ASTM Standard E23 untuk ujian hentaman Charpy dan ASTM E8 untuk ujian tegangan dan standard yang sama turut digunakan untuk ujian makmal masing-masing. Spesimen Charpy telah difabrikasi dengan ketebalan berbeza 5mm, 7.5mm dan 10mm dengan menggunakan Pencetak 3D Ermaksan Enavision 120 SLM. Pemilihan parameter kajian ini ialah 230V, kelajuan imbasan 5m/s, kelajuan imbasan 32A, 300W, argon dan nitrogen sebagai gas lengai, dan paras oksigen 2500 ppm. Ujian Kesan Charpy ke atas spesimen dilakukan ke atas sampel rata dan perbandingan bahan seterusnya kerap dijalankan terhadap keputusan yang diperoleh daripada ujian impak yang dilakukan menggunakan spesimen Charpy. Tenaga yang diserap, isyarat tolok terikan dan ujian tegangan menghasilkan bahan kekuatan S 316 L-A11. Keputusan menunjukkan bahawa spesimen S 316 L-A11 dengan ketebalan 10.0mm mempunyai nilai tenaga serapan yang lebih besar. Kawasan di bawah graf terikan-masa, terikan maksimum dan tenaga yang diserap semuanya dipengaruhi dengan ketara oleh ketebalan spesimen. Kajian ini juga membuat perbandingan antara graf masa terikan antara S 316 L-A11 dan SS3304. Hasil perbandingan menunjukkan bahawa S 316 L-A11 adalah bahan yang lebih disukai untuk digunakan dalam pembuatan bahan tambahan kerana kekuatan bahan.

ACKNOWLEDGEMENTS

TABLE OF CONTENTS

.

LIST OF TABLES

LIST OF FIGURES

viii

LIST OF SYMBOLS AND ABBREVIATIONS

2D	-	2-Dimensional
3D	-	3-Dimensional
STL	-	Stereolithography
CAD	-	Computer-Aided Digital
SLM	-	Selective Laser Melting
ALM	-	Additive Layer Manufacturing
ASTM	-	American Society for Testing and Materials
SLS	-	Selective Laser Sintering
EBM	-	Electron Beam Melting
L-PBF	-	Laser Beam-based PBF
PBF	-	Powder Be Fusion
DMLS	-	Direct Metal Laser Sintering
DED	-	Directed Energy Deposition
mm	-	millimeter
μm	-	micrometer
US	-	United States
UK	-	United Kingdom

LIST OF APPENDICES

UNIVERSITI TEKNIKAL MALAYSIA MELAKA

xi

CHAPTER 1

INTRODUCTION

1.1   Background

The development of 3D printing technology is reaching an unprecedented pace. Using this method, complex geometric parts can be generated directly from computer-aided digital (CAD) files, which are later converted to stereolithography (STL) files. In this process, drawings created in CAD software are approximated and sliced into triangles containing information for each layer to be printed. The advantage of additive manufacturing is that it allows the construction of internal features that are difficult to manufacture using traditional methods. In the SLM process, products are created by selectively melting successive layers of powder through the interaction of a laser beam. During irradiation, the powder material is heated and, when enough power is applied, melts to form a pool of liquid. The molten pool then solidifies and cools rapidly, and the solidified material begins to form the product. After the layer cross-section is scanned, the construction platform is lowered by an amount corresponding to the layer thickness and a new powder layer is applied. This process is repeated until the product is completed (Kumar et al., 2021).

On the other hand, SLM still has obvious limitations in surface quality compared to alternative metal manufacturing processes such as machining. The quality of the surface is greatly influenced by the "staircase effect" in which curves and slopes gradually approach each other. This effect is present to a greater or lesser extent in all

additive layer manufacturing (ALM) processes as a result of the additional deposition and generation of layers. Despite the fact that the layer thickness can be reduced to improve the surface finish, obtaining a good surface finish is a very important issue in SLM manufacturing. The complexity of the shapes of manufactured parts reduces the benefits of using additive manufacturing processes in industrial production especially in automotive industry (D.A. Lesyk et al., 2020).

During the SLM process, the build chamber is often filled with nitrogen or argon gas to create an inert atmosphere and protect heated metal parts from oxidation. Additionally, some SLM machines can preheat the substrate plate or the entire build chamber. The layer thickness is typically 20-100 μm. This is chosen to balance achieving fine resolution with good powder flowability. Powders with large particle sizes have poor resolution and buildup resistance, and small powders tend to aggregate easily due to van der Waals forces. Therefore, if the powder fluidity is low, the powder separation will be poor.

1.1.1   Additive Manufacturing

As technology continues to advance, additive manufacturing is poised to play a pivotal role in reshaping the future of manufacturing by unlocking new possibilities in design, production efficiency, and material utilization. Additive manufacturing often referred to as 3D printing, is a revolutionary manufacturing process that has transformed traditional methods of creating objects and components. Unlike subtractive manufacturing, which involves cutting or shaping material to achieve the desired form, AM builds objects layer by layer, directly from digital models. This innovative technique allows for

unparalleled design flexibility, enabling the production of complex geometries and intricate structure that would be challenging or impossible accross various industries, including automotive, aerospace and consumer goods, offering advantages such as reduced waste, faster prototyping, and the ability to produce customized, on demand products.

Other than that, Solomon et al. (2016) stated that the physical part of a smart factory is limited by the performance of existing manufacturing systems. This makes AM a central component of Industry 4.0. Industry 4.0 requires the development of non-traditional manufacturing methods due to the need for mass customization. AM therefore has the potential to become a key technology for producing customized products, as it can produce sophisticated objects with advanced properties (new materials, geometries). Due to improved product quality, AM is now used in a variety of industries including automotive, aerospace, and manufacturing. Although there are still questions about its applicability to mass production, new technological advances are increasing the use of AM in industry. It is an evolving technology to increase production speed and produce complex objects with precision and stability, and thus may provide an alternative to traditional manufacturing techniques in the near future. Hence, more recently the American Society for Testing and Materials (ASTM) group "ASTM F42 – Additive Manufacturing" (2010) has formulated a set of standards that classify the range of Additive Manufacturing processes into seven categories (Standard Terminology for Additive Manufacturing Technologies, 2012) as illustrated in Figure 1.1.

Process types	Brief Description	Related Technology	Companies	Materials
Powder Bed Fusion	Thermal energy selectively fuses regions of a powder bed	Electron beam melting (EBM), selective laser sintering (SLS), selective heat sintering (SHS), and direct metal laser sintering (DMLS)	EOS (Germany), 3D Systems(US), Arcam (Sweden)	Metals, Polymers
Directed Energy Deposition	Focused thermal energy is used to fuse materials by melting as the material is being deposited	Laser metal deposition (LMD)	Optomec (US), POM (US)	Metals
Material Extrusion	Material is selectively dispensed through a through Nozzle or orifice	Fused deposition modelling (FDM)	Stratasys (Israel), Bits from Bytes (UK)	Polymers
Vat Photo polymerization	Liquid photopolymer in a vat is selectively cured by light-activated polymerization	Stereo lithography(SLA), digital light processing (DLP)		Photopolymers
Binder Jetting	A liquid bonding agent is selectively deposited to join powder materials	Powder bed and inkjet head (PBIH), plaster-based 3D printing (PP)	3D Systems (US), Ex One (US)	Polymers, Foundry Sand, Metals
Material Jetting	Droplets of build material are selectively deposited	Multi-jet modelling (MJM)	Objet (Israel), 3DSystems (US)	Polymers, Waxes
Sheet Lamination	Sheets of material are bonded to form an object	Laminated object manufacturing(LOM), ultrasonic consolidation (UC)	Fabrisonic (US), Mcor (Ireland)	Paper, Metals

Figure 1.1 Seven classes of AM

1.1.2 Selective Laser Melting (SLM)

Four out of seven AM methods can be used to make parts that made of metallic materials, however, one of the process that proffer numerous possible benefits among the seven AM methods is the Powder Bed Fusion (PBF) process. The process is among the ones which are getting increasing attention as an emerging polymer and metal AM technology, and it uses laser or electron beam as an energy source for fusing or melting the powder materials to create parts layer-by-layer (C. Liu et al., 2020). SLM is one of the example of beam-based PBF process. PBF procedures are divided into two categories: non-beam (heater/lamp)-based PBF, which does not require a high energy beam, and beam-based PBF, which needs a high energy beam. Beam-based PBF techniques include Selective Laser Sintering (SLS), Selective Laser Melting (SLM), and Electron Beam Melting (EBM). There are two types of beam-based PBF processes: electron beam PBF

15

process, which includes EBM process, and laser beam-based PBF process (L-PBF, which includes SLS and SLM processes). Selective Laser Melting (SLM), a well-known AM method that falls under the L-PBF category, creates nearly net-shape objects with complicated geometries, good mechanical properties, and a smooth surface appearance.

The method, which involves melting metallic powders using a high-power density laser, is suitable for creating multifunctional objects with a higher density of up to 99.9%. The SLM process, as seen in Figure 1.2, starts with the application of a small layer of powder on the construction platform, which melts completely when one or more laser beams provide thermal energy. The need for the SLM process is rapidly growing in a number of industries, including aerospace, automotive, electrical, chemical, biomedical, and other high-tech fields, because of its mechanical properties and lightweight features. In the automotive sector, one of the most useful SLM procedures is for creating complex-shape components (e.g automotive steering housing gear) from a variety of materials, such as steel, titanium alloys, and superalloys based on nickel. Additionally, these procedures can improve the part's weight and reduce the number of assembly pieces into a single component . In the meantime, shrinkages and residual stress are important SLM process phenomena. During the process, the material gets larger because to the laser power, and if that power is removed, it will shrink. Furthermore, the residual stress was also a result of using the incorrect process parameters.
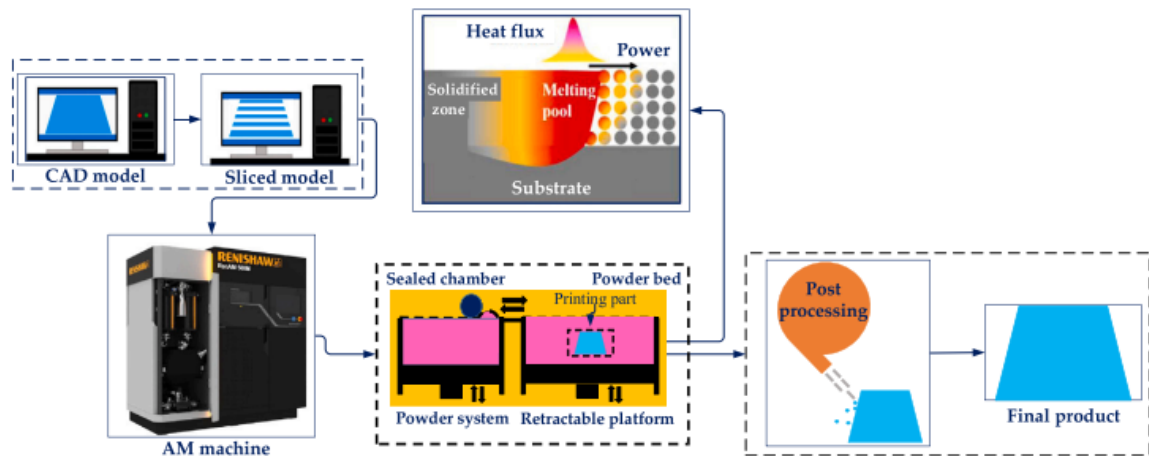
Figure 1.2 Working principle of SLM process

1.2   Problem Statement

Selective Laser Melting (SLM) has becoming a well-established method for producing complex shaped parts in typical impact test on pipes are performed on curved samples, and subsequent materials comparison are frequently conducted against results obtained from flat samples. Although many studies have been conducted concerning non-standard Charpy V-Notched specimens, none have addressed the influence of specimen curvature on impact test results.

1.3   Research Objective

The main aim of this research is to study the strength material for additive manufacturing on impact tests. Specifically, the objectives are as follows:

a) To study the impact and tensile strength test using 3D printer metal specimens.

b) To investigate the Charpy impact test with different thickness and orientation.

c) To compare absorbed energy, strain signal pattern between 3D metal printer material and normal material using Charpy impact.

1.4   Scope of Research

The scope of this research are as follows:

- Specimens produced for this study are limited by using S 316 L-A11 powder.

- Specimens are printed by SLM processs through a 3D printer machine call ed Ermaksan Enavision 120 SLM.

- Analyze previous research about specimen strength material at different thickness (5.0mm, 7.5mm, and 10.0mm).

- Performing Charpy Impact Test, Strain signal and Tensile Test to get the strength material of specimens.

- The ASTM E23 is standard test method for notch bar impact testing of metallic materials.

- The ASTM E8 is standard test method for tensile test.

CHAPTER 2

LITERATURE REVIEW

2.1   Introduction

A literature review was conducted in this chapter to gather information of previous studies to complete this project. Previous related resources from journals or articles are the primary resources, meanwhile related resources from internet and books are among the secondary resources that are used for this project. In this chapter, there are findings on type of materials used, SLM process, thickness variations in 5.0mm, 7.5mm and 10.0mm.

One of the most important technologies for the direct formation of metal parts in 3D printing is selective laser melting (SLM). Direct formation of items with complicated shapes, great dimensional precision, and superior mechanical qualities is possible using SLM technology. In particular, appropriate for the quick production of specialized and bespoke structures made of challenging-to-machine automotive elements. Complex material physical and chemical behavior is involved in the SLM forming process. The forming mechanism differs significantly from conventional casting methods. The parameters of the procedure are intricate and challenging to regulate (Li-Ii Jing, 2020).

The test used to do the impact test is the Charpy Impact Test. Charpy method involves striking an appropriate test material with a striker fastened at the end of a pendulum. The test material is secured horizontally in place at both ends, and the striker hits the center of the test material, behind a machined notch. The notch is positioned

away from the striker, fastened in a pendulum. The test material usually measures 55×10x10 millimeters. The Charpy method has a machined notch across one of the larger faces. There are two types of charpy notch, a V-notch or a U-notch. The V-notch, or the AV-shaped notch, measures 2 millimeters deep, with a 45 degree angle and 0.25 millimeter radius, parallel to the base. The U-notch, or keyhole notch, is 5 millimeters deep notch, with a 1 millimeter radius at the bottom of the notch. Higher speeds and collision energy could be achieved in a vertical style fall. This method proved to be reliable, and gave qualitative collision data.

2.2   History of Selective Laser Melting (SLM)

Looking back at the SLM technique's development history, it was originally intended to merge conventional processing with selective laser melting (SLS) technology (Kruth J. Et al., 2004). In 1986, Deckard C., a graduate student at Texas University studying Austin Distribution, proposed the concept of SLS technology. Many people at the time examined this technology in great detail since they were very interested in it. The world's first SLS machine was created in 1988 (Y. Tang et al., 2003). The DTM Company of the United States joined the public company 3D Systems of the United States in 1992. A commercially viable SLS device has been created by United States. High power laser technology is still developing and typically somewhat costly in the early stages of SLM technology development.

Simultaneously, the limited capabilities of computers cannot satisfy the demands of huge data control. As a result, SLS technology and metal powder coating were used in the early stages to indirectly produce metal parts (Kruth J.). The cost of producing lasers has

drastically decreased thanks to advancements in laser manufacturing technology, and computer performance has been steadily rising. The SLM technology of laser totally melting metal powder formation was initially investigated by the Fraunhofer Institute for Laser Technology (ITL) in Germany. The technique was soon developed by EOS in Germany. By the end of 1994, the first SLM equipment was manufactured with support. Following that, a large number of businesses from the US, UK, and Germany started manufacturing commercial SLS equipment (R. Morrgan et al., 2004).

2.3   Current challenges on AM

The challenges that AM software is currently facing are a result of the technology's relatively new introduction and radically changed production process. As previously said, subtractive methods have dominated traditional manufacturing and have encouraged the creation of simple parts to save tool changes and production costs.

In contrast, AM encourages the creation of more organic forms and structures because the intricacy of a part does not affect the cost or time required for production. Even though this is one of AM's main benefits, it is now difficult to realize AM's full potential because standard CAD programmes cannot produce these freeform models with ease.

Accurately simulating the AM process and producing findings that can be put into analytical models is currently quite difficult because CAD programmes were largely built for subtractive procedures. Thus, trial-and-error methods—which are expensive and time-consuming—are frequently used to validate and improve part designs (M. M. et al.,2017).

21

The fact that various software packages are currently needed for the entire design process is another major problem with AM software. The creation, optimization, and verification of a model are necessary first steps that usually demand the use of a variety of software applications, such as CAD, topology optimization, and CAE. After taking these actions, different programmes are needed for the stages of build verification and build preparation in order to produce the 2D slice data that the AM machine will need. In addition to being cumbersome, this reliance on distinct software packages at various phases of the model design and preparation process is restricting since it is difficult to move data between different programmes, which can result in model approximations and data loss (Kozak et al., 2021).

2.4   Powder Bed Fusion (PBF)

PBF is a class of additive manufacturing (AM) technologies in which powder particles are selectively bonded or melted using an energy source to construct things layer by layer with the required geometry. Selective laser sintering (SLS), the original PBF method, was created at the University of Texas. SLM started in 1995 at the Fraunhofer Institute ILT in Aachen, Germany (Ahmadi et al.).

The latter basic technique is substantially altered by all other PBF procedures in one or more ways to increase machine productivity. Figure 2.1 shows the fundamental schematic representation of the PBF process. PBF is a commonly used and potentially the most advanced AM technology accessible. As of 2020, PBF procedures account for 54% of the metal AM market (Vafadar et al.). PBF-process is the most advanced metal AM method for producing engineering components. (Korpela et al.). The manufacturer of

PBF machines goes by distinct trade names, including SLS, direct metal laser sintering (DMLS), and SLM, which stands for electron beam melting (EBM) or laser powder bed fusion (L-PBF). The bulk of metal PBF systems in use today totally melt the particles rather than sintering them, despite the fact that certain systems contain the word "sintering" in their titles.
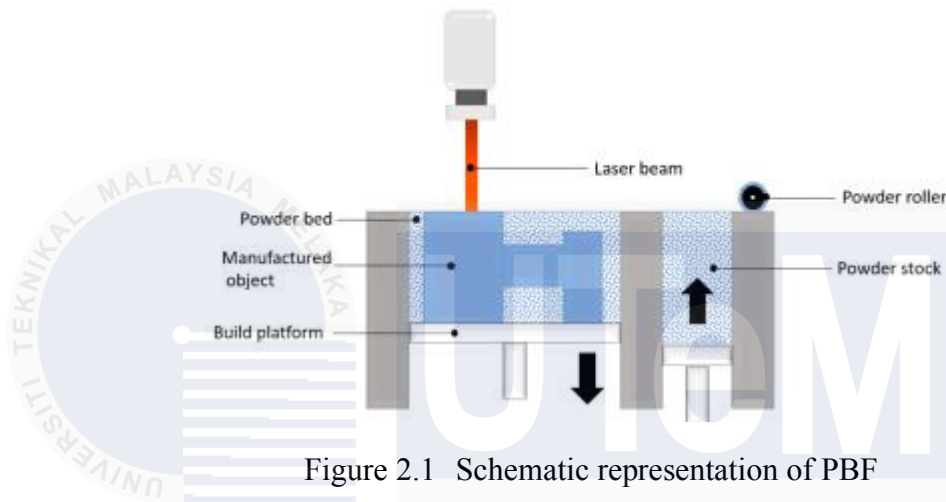
Figure 2.1   Schematic representation of PBF

A growing area of study is comparing the efficacy of PBF and other procedures. For instance, the PBF and directed energy deposition (DED) have similar characteristics. The PBF system makes use of a powder deposition technique that includes a powder reservoir and a substrate plate that are coated with powder via a recoating mechanism. Once the powder is equally spread, PBF traces the geometry of each layer of slices from a 3D model on the surface of the powder bed using thermal energy from a heat source (an electron beam or a laser).

The energy and feedstock sources that PBF uses can also be used by DED. On the other hand, DED uses a nozzle to apply melted material feedstock to a surface. The resemblance between PBF and DED while using the same energy source turns into a thought-provoking issue. Because PBF is a slower process, DED has a higher deposition

rate and is therefore preferred for making larger components. When it comes to creating

parts with more resolution and quality than DED methods, PBF methods are superior.

The previous study claimed that PBF and DED under a laser beam create the mechanical

performance of Fe-Co components—are supported by Babuska et al.'s findings. While L-

DED produces low strength (200–300 MPa) and poor ductility (0–2.7%), the part L-PBF

was described as having high strength (500–550 MPa) and high ductility (35%).

2.4.1 Selective Laser Sintering (SLS)

One of the earliest Powder Bed techniques to be commercialized, SLS set the

groundwork for PBF's ongoing growth. Based on this approach, all PBF processes have

been adjusted to improve productivity and allow for the creation and use of various

materials. Figure 2.2 provides an example of the procedure. As was previously said, the

procedure consists of the scanner first scanning the areas, after which the laser is guided to

build the first sintered layer. The roller is then used to spread the second layer over the

first, adjusting the thickness of each layer as it goes. With the help of the scanner's helium

p, the laser then fuses the layers.
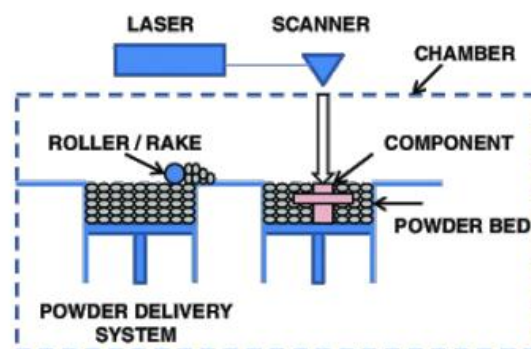
Figure 2.2 Description of the different parts of the laser beam powder
bed fusion process

24

2.4.2 Selective Laser Melting (SLM)

SLM differs from SLS in that it permits the use of metals with high melting points. The primary distinction is that it melts rather than sinters the alloy powder. Since the alloy powder is being melted, this also permits a larger microstructure and offers substantially better mechanical qualities than SLS.

2.5 Advantages and Challenges of L-PBF

Because AM and its subcategories build products layer by layer, waste is eliminated during the process, allowing for a large degree of creative design freedom. The manufacturing of both polymer and metal items is made possible by powder bed fusion technology, which expands the scope and liberty of the designer. Because there is no need to take into account tools and tool pathways, topology-optimized design—a technique for minimising volume—allows for the delivery of superior precision and product quality than subtractive design while also saving weight and materials. L-PBF technology is one of the largest issues because it is more expensive in terms of time and resources than subtractive manufacturing, particularly when there is already an efficient subtractive method of manufacturing the detail.

To operate the equipment and the powder itself safely, L-PBF needs the operator to have a thorough understanding of both the material and the machines. Since the powder utilised in these devices is typically between 25 and 45 μm, producing L-PBF in a clean environment is necessary to ensure operator safety. The expense of this creates significant hurdles for many sectors. Additionally, the size of the part is limited by the machinery.

Although larger L-PBF systems have a build capacity of up to 500 x 280 x 850 mm, their application is still restricted to larger parts or mass manufacturing.

2.6   S 316 L in Automotive Industry

In current automotive industry, stainless steels are widely especially in motor vehicle applications because the ability of the metal to resist corrosion and high temperature oxidation, offering absorbed energy properties and sustain its mechanical properties over a wide temperature range. According to International Stainless steel Forum (ISSF), automotive industry puts the usage of stainless steel as the key structural components.

The purpose of stainless steels (SS), which are iron-based alloys with at least 10.5% chromium (Cr), is to stop rust (Milano et al., 2014). In order to produce the invisible and adhering chromium oxide surface coating on the surface of a stainless steel that offers corrosion resistance and inhibits further oxidation, some stainless steels have more than 30% of Cr or less than 50% of Fe (Park, 2005).The low carbon form of stainless steel 316 (SS 316) is known as stainless steel 316L (SS 316L). The standard grade SS316L, which contains molybdenum, provides greater creep, stress to rupture, and tensile strength at higher temperatures than grade SS 316 (S. Frashetti et al., 2005). Applications for stainless steel 316L in the automotive industry include baggage racks, handrails, turbocharger housings, and catalytic converter housings are as shown in Figure 2.3. This is due to its high temperature applications, durability and corrosion resistance at low cost (K. C. Taylor, 1987).

Figure 2.3   Examples of automotive parts made of S316L

2.7   Argon Gas and Nitrogen Gas

Suitable type of gases used for SLM process is very important as the scope of process of SLM is limited to argon gas and nitrogen gas. Figure 2.4 shows gas that been used in this study. Argon is a type of noble gas while nitrogen gas considers as molecule which can dissociate with other type of gases like oxygen, hydrogen and sulphur. These gases also can dissolve in molten metal including nitrides with active metals. The type of gases use in SLM plays significant role as protection from occurance of oxidation. The temperature increases significantly when the powder bed interacts with the laser beam and the formation of stable oxides occured. Required atmosphere purity established by flushing the process chamber volume with the selected gas to protect the material from oxidation. The flushed gas is then vented out. Any presence of oxygen and impurities in the chamber will be diluted. This process continues until the machine detects less than a given oxygen level and begin to recirculate the gas.

Figure 2.4 Type of gas used in SLM process (oxygen, O₂)

2.8   Mechanical Properties

Though they have a slightly different meaning when applied to lattice structures than when applied to continuous bulk materials, terminology such mechanical characteristics, elastic modulus, and yield strength are nevertheless used to describe them. These characteristics are known as the "apparent macroscopic properties of structures that converge to certain values when the number of the unit cells is large enough" (A. A. Zadpoor, 2018) in relation to lattice structures. Lattice structures can achieve mechanical or functional properties that bulk materials cannot match because of the geometric freedom that AM provides (P. Koehman, et al., 2018). Examples of these properties include auxetic structures with negative Poisson's ratio (S. Babaee, et al., 2013), negative stiffness (E. B. Duoss et al., 2014), negative compressibility (J. N. Grima, et al., 2011), negative thermal expansion coefficient (Q. Wang, et al., 2016), or very high stiffness with low mass (X. Zheng, et al., 2014).

The relative density of the lattice structure, which is the ratio of the apparent density of the cellular structure to the density of the cellular structure's material,

28

determines the mechanical properties of lattice structures, which are typically expressed as a fraction of the mechanical properties of their parent material (A. A. Zadpoor et al., 2018). The mechanical characteristics of lattice structures are known to decline with lower relative density, regardless of topology (H. E. Burton, et al., 2019). The mechanical response of anisotropic lattice constructions is also strongly influenced by the orientation of the cells about the direction of loading.

Because compression testing is easier to do than tension testing, most of the mechanical testing for SLM lattice structures is done in this manner. This is mainly because compressive tests may be carried out more easily by crushing a lattice between plates, but tensile testing requires design of the sample-test equipment interface. For instance, observed that lattice structures failed close to the interface where the lattice structure and test apparatus connection met, indicating the presence of a critical stress concentration at the lattice interface when testing lattice structures under strain (H. Alsalla et al., 2016). There is still need for more study in lattice structure tensile behavior.

The mechanical property of material defines the behavior of the material when subjected to external force or also known as loads. Mechanical properties can also be used to identify and categorize metals. Absorbed energy, strain signal and yield strength are the most common properties that have been analyzed.

2.8.1   Impact Test

The Charpy Impact Test samples were fabricated based on ASTM E23-18 (Rafieazad et al., 2021). An impact testing machine with a maximum capacity of 500 J

29

has been used for this study. The absorbed energy during fracture by each specimen were measured at three different thicknesses; 5.0mm, 7.5mm and 10.0mm which each specimens have five samples respectively. The energy absorbed in the specimen's fracture was measured when the Charpy impact test machine's pendulum strikes the specimen positioned between the anvils. This is a straightforward method of determining the impact toughness of metal (Iowa, 2008).
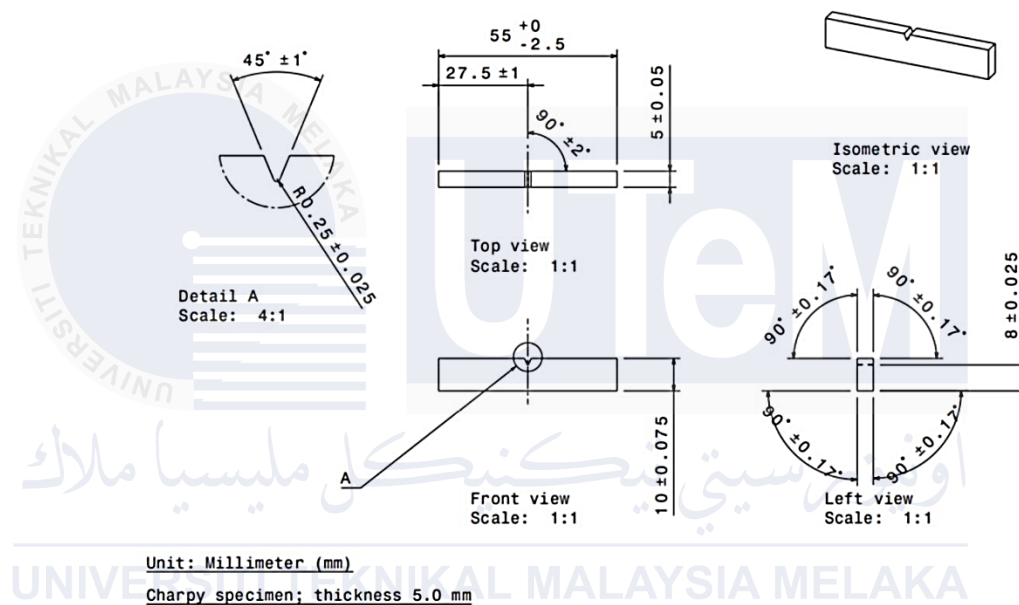
Figure 2.5 Charpy impact test specimen dimension size

The horizontal, vertical, and 45-degree orientations of the impact test specimens are illustrated in Figure 2.5. The materials' toughness is the area under the stress-strain graph. The Charpy impact test repeated five times for each specimen. At different thickness, the material has varied impact toughness, and it is more brittle while at lower thickness, therefore, it is more ductile.

30

The fracture surfaces of every specimen just after the Charpy impact test are shown in Figure 2.6. The specimens as received display the smooth fracture surface morphology as shown in Figure 2.6(a), where the crack begins at the apex of the notch and proceeds downward properly (Mandal, 2019).

The features of the ductile fracture are similar to those of this kind of fracture. The specimen has been restored, but the brittle fracture shape is still visible. In specimens that have been repaired, the fracture initiates at the notch's tip and attempts to spread in these directions as it descends towards the substrate, where it encounters several flaws. The crack could not propagate very far throughout the restored specimen because the faults are not strong enough to support it.

Ultimately, the final fracture occurs as the crack contacts the interface between the substrate and the deposited area and begins to propagate across that interface across the specimen. expressed as Figure 2.6(b). The fracture surfaces of a fully AM-fabricated subsize specimen and the repaired subsize specimen are depicted in Figure 2.6(c-d), respectively. Both AM (subsize) and RS (subsize) have brittle fracture properties, meaning that their fracture surfaces are not smooth. The behavior of RS (subsize) is comparable to that of the other repaired specimens.
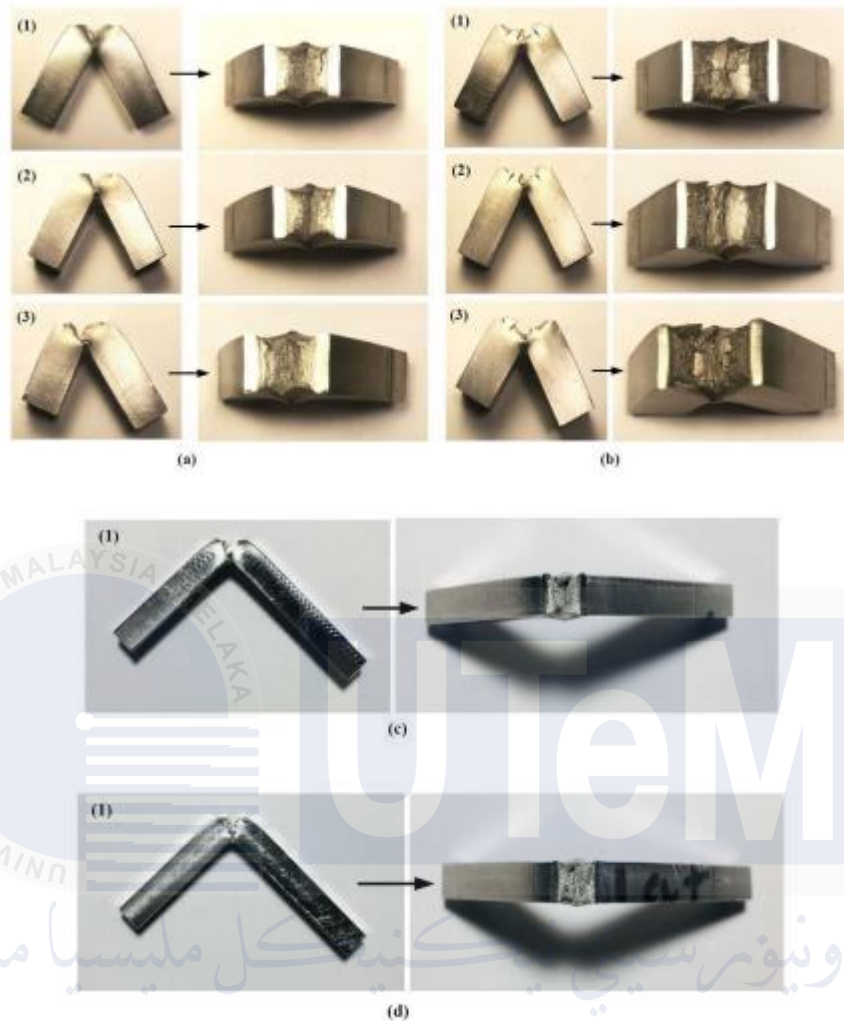
Figure 2.6   Fracture surface images of (a) as-received specimen (b) repaired specimen (c) AM (subsize) specimen (d) repaired (subsize) specimen. [AR= As-Received; RS= Repaired Specimen; AM=Additive Manufactured]

2.8.2   Strain Signal

Because it is inexpensive and dependable, the Charpy impact test has been researched and used extensively over the years. It is still one of the techniques used to investigate the fracture toughness problem. The Charpy v-notch test, a standardized high strain rate test, is used to determine the amount of energy absorbed in a material. The absorbed energy, which is measured using a dial/encoder system, is thought to be a good

indicator of a material's toughness and can be used to predict the ductile-brittle transition depending on the testing temperature. The goal of using the load-time recording system in conjunction with the instrumented Charpy impact apparatus is to ascertain the fracture energy and general yielding of material. the highest weight that was placed on the samples. and lastly, the brittle fracture occurrence moment level (2-4). To measure the absorbed energy during the impact, a standard Charpy test instrument has an optical encoder and a dial indication.

Overall absorbed energies measured with different technologies are normally quite similar, though occasionally notable variations in quantity can be observed. Using an optical encoder or dial indicator, the total absorbed energy has been determined to be either higher or lower depending on the specimen thickness, ductility of the test specimen, and other parameters. More than 80% of the absorbed energy is estimated and not entirely precise (Xu et al.).

Meanwhile, an accelerometer and strain gauges linked to the impact striker have been used to experimentally analyses the dynamic reactions from a conventional Charpy impact instrument; the findings of this study have also been verified using finite element analysis. Despite differing with strain gauges, the initial natural frequencies in the acceleration signal of the Charpy sample in that investigation had high modal magnitudes. When Toshiro et al. examined the position of the strain gauge and the impact of the striker shape on an instrumented Charpy impact test, they discovered that the hammer vibration appeared to have a greater effect near the end of the slit.

Different materials having contact stiffness, such as the specimen and the striker, were explained by Sahraoui and Laitailate. Furthermore, they discovered that the specimen-striker interaction plays a major role in the vibration and impact effects by employing a particular approach to assess the load oscillation frequency.

Additionally, during the fracture toughness testing, Kondryakov et al. investigated a multichannel system of high-speed strains and loads recording method. with the strain gauges fastened to both the specimen support and the striker. Their method made it possible to record data about specimen deformation that happened during the test. Francois and Pincau investigated an observation regarding discrepancies between dial/encoder energy and the energy measured by U-hammer on instrumented strikers.
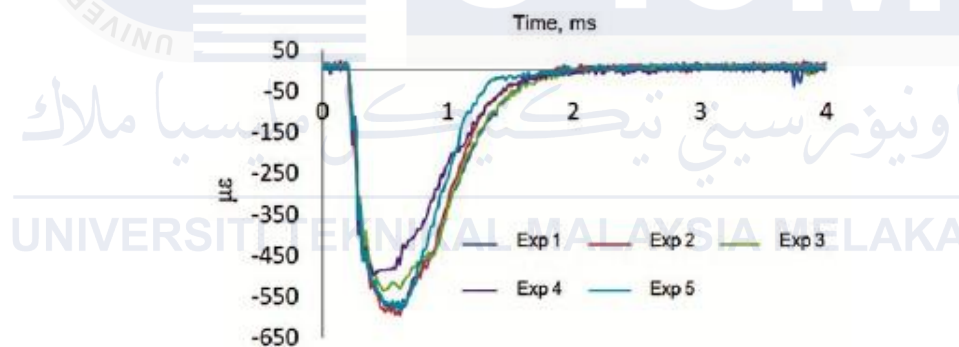

Figure 2.7 Example of time history of strain signal

2.8.3 Tensile Test

One of the best and possibly most basic techniques for determining a material's mechanical characteristics is to perform tensile testing. A test coupon is inserted into a machine that pulls on the material until the test is finished, which often occurs when the test coupon breaks. With the test coupon's geometry taken into consideration, the

34

machine's time, load, and displacement data can be utilized to generate an engineering stress-strain curve.

The ASTM E8 Standard Test Methods for Tension Testing of Metallic Materials specification was followed for all baseline tensile testing in this study. The geometry of the subsize plate-type tensile specimen in use is depicted in Figure 2.7 below.

Pressing Area =1.00 in.²
Dimensions Specified, are Those of the Die
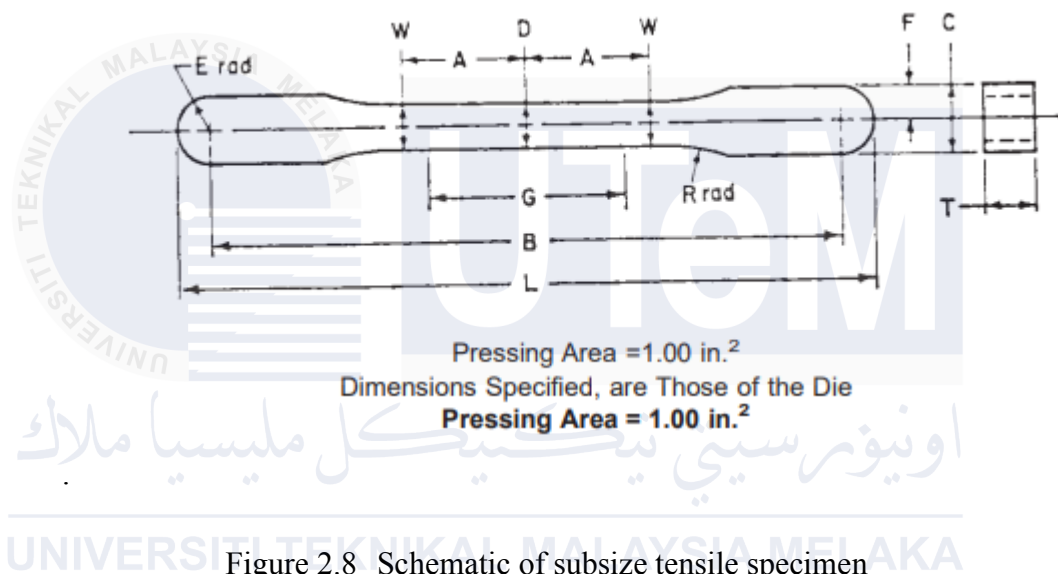**Pressing Area = 1.00 in.²**

Figure 2.8 Schematic of subsize tensile specimen

Previous study had conducted to study the tensile test of additive manufacturing specimens where six distinct FDM filaments were examined for the analysis. Comparing the tensile strength characteristics of PLA (polylactic acid)-based composites with various additive materials was our aim. Two distinct approaches were employed: first, the test specimens for tensile stress were compared, and then each filament material's stress characteristics were examined. The outside diameter of each thread was 1.75 mm during the tests. A Cetus MKII extended 3D printer was used to carry out the printing. When printing the first wave of test specimens, the printer was set to its default settings, with 100% filling. The 4 mm thick printed tensile strength test specimens were produced in compliance with the

ISO 3167 1994 standard (Varga L. et al., 2018). An Instron 5566 type tensile machine was used to conduct tensile tests. At room temperature, the measurements were done at a pace of 50 mm per minute. The details of the specimen are shown in Figure 2.8.
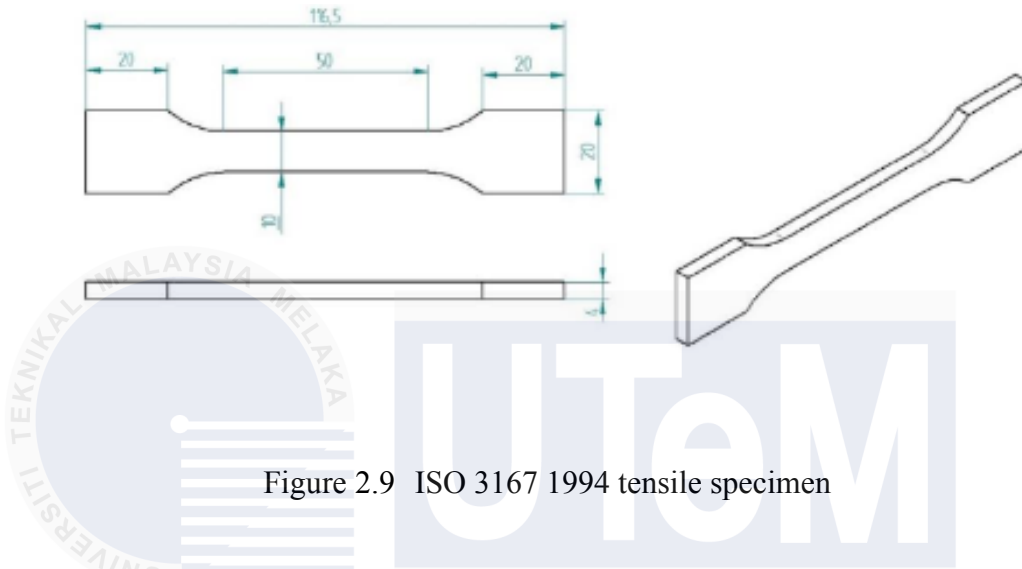

Figure 2.9   ISO 3167 1994 tensile specimen

Figures 2.9 and 2.10 provide a summary of the experiment results. It is evident that the printing process weakens the material; that is, when an additive is present in the material, the printed specimen's tensile strength is lower than that of the original filament thread.
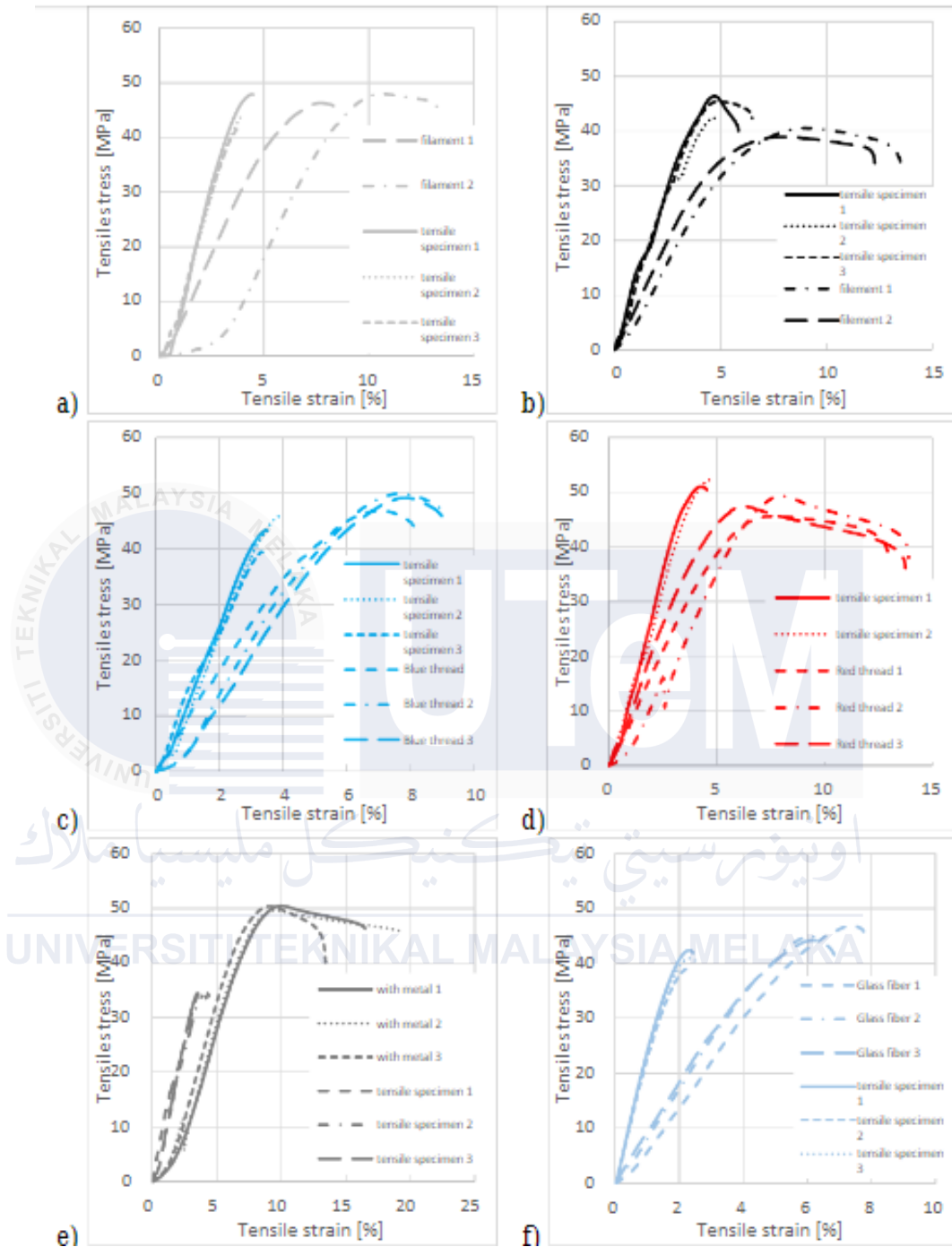
Figure 2.10   Tensile test result of a) chalk powder, (b) "technical", (c) 5% glass fiber, (d) basic PLA, (e) 10% metal powder, (f) glass fiber filament
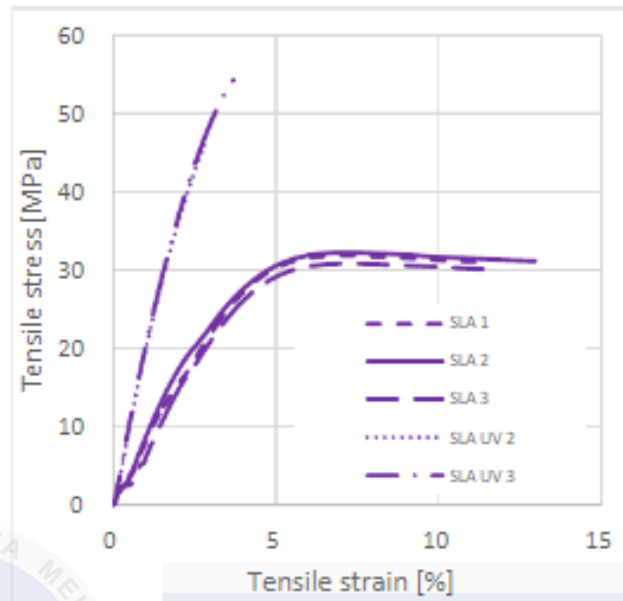
37

Figure 2.11   Tensile test result: SLA

The test findings are condensed into a single graphic in Figure 2.10. Data on tensile stress ranges from 38 to 50 MPa for every test material. Given that the result falls within the range of values reported in the literature (Varga L. et al., 2018).
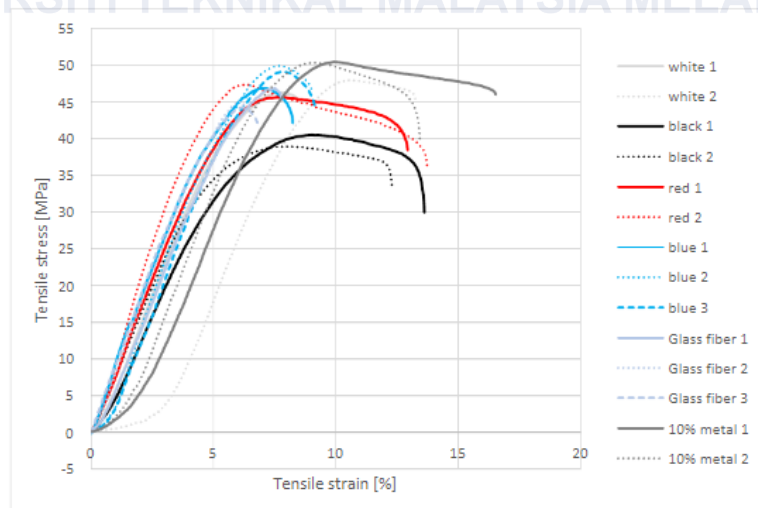

Figure 2.12 Tensile test: result of all filaments

METHODOLOGY

2.9 Introduction

In this chapter, the specimens were produced by using Ermaksan Enavision 120 SLM 3D Metal Printer. The details of testing procedures, investigation methods and data analysis techniques are explained in this chapter. This study process and testing are based on discussions and research conducted by previous researchers.

2.10 Flowchart

The project sequential phases are shown in a process flowchart including the decisions taken for each of the process to work. The primary actions of the research methodology is illustrated in Figure 3.1. Each step in the flowchart is represented by a certain shape accordingly. Lines and arrows are used to indicate the flow or the movement of this study. The metal powder used for this study is S 316 L-A11 and three different specimens thickness are used in this test are 5.0mm, 7.5mm, 10.0mm. To conclude, the specimens are prepared by Selective Laser melting (SLM) process accordingly to get specific requirements to run the specific test which are Charpy Impact Test, Strain Gauge Signal and Tensile Test.
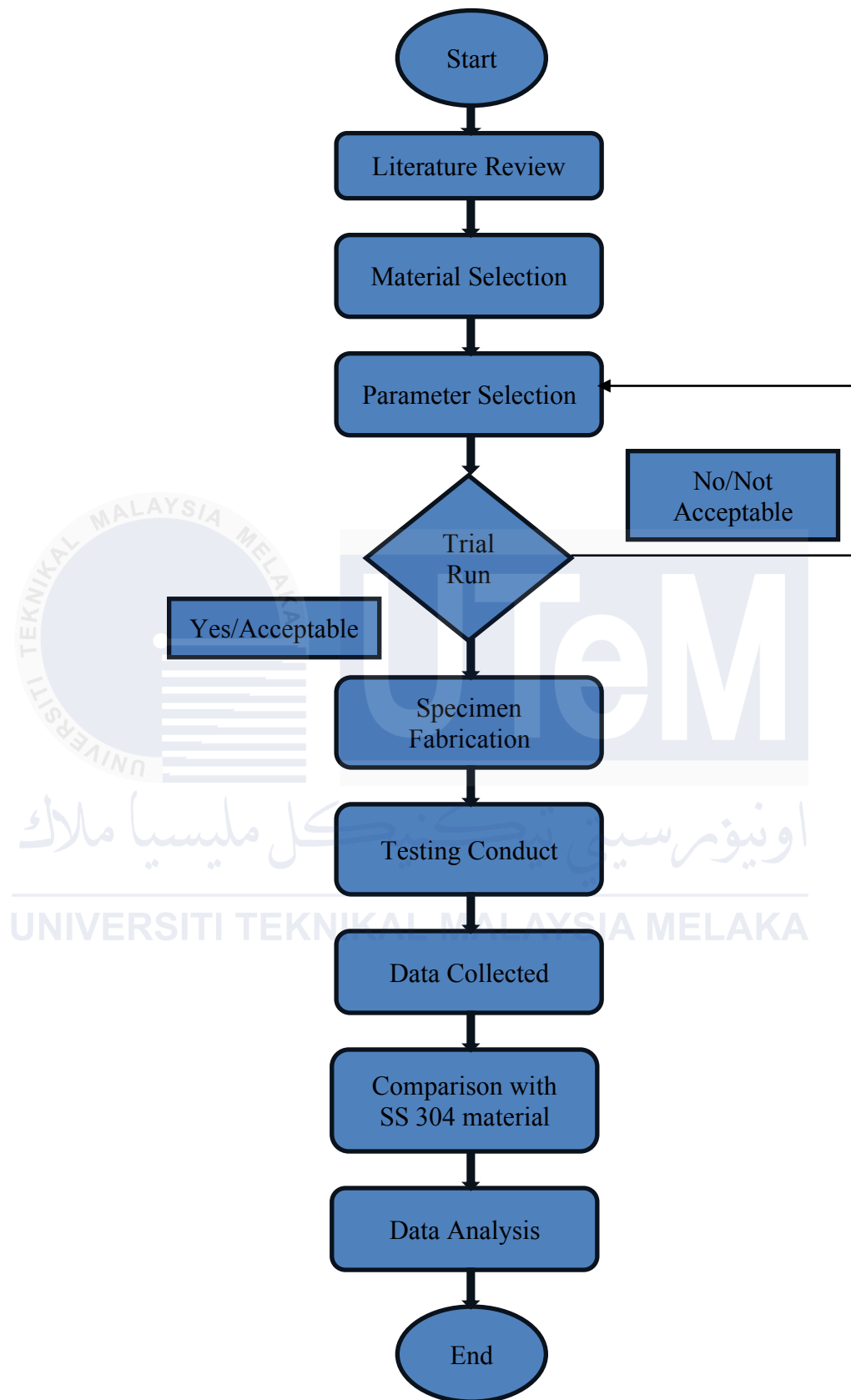
Figure 2.13   Flowchart of research methodology

2.11 Material Selection

In this experiment, only one type of material is used to conduct the all the tests. The material used is S 316 L-A11 powder, argon and nitrogen are the type of gases used in this experiment.

2.11.1 Stainless Steel (AISI 316)

Since the 1930s, a single car has typically required the use of 15 to 22 kilograms of stainless steel, mostly for the exhaust system and other tiny components. Stainless steel is being used in a wider range of automotive applications, including brackets, flanges, substructures, panels, fasteners, springs, and tubing. As time went on, more and more stainless steel varieties, including austenitic, martensitic, ferritic, and many others, were developed, bringing the cost of wielding closer to what it is today. Because of its long endurance and ease of welding, austenitic stainless steel emerged as the best type of stainless steel for usage in the automotive sector. AISI 316 is the most typical stainless steel used in various production in automotive, aerospace and also biomedicals. The characteristics and properties of stainless steel are depending on the composition, but in general, stainless steel have low percentage of carbon and gives it to be superior resistance to corrosion. Tensile strengths are typically around 500 to 700 MPa, with typical elongation from 30% to 50%. Table 3.3.1 shows the chemical compositions in 316L which is an austenitic stainless steel alloy that suitable for marine and industry settings (Vishwa, 2022).

Table 1 Chemical composition of AISI 316 Stainless Steel

Element	Composition
Chromium	16 % - 18 %
Nickel	10 % -14 %
Molybdenum	2 % - 3 %
Manganese	1 %
Silicon	1 %
Carbon	0.03 %
Sulfur	0.03
Phosphorus	0.045
Iron	Balance

2.11.2 S 316 L

The common molybdenum-containing grade, 316, is ranked second among austenitic stainless steels, after 304. Compared to Grade 304, molybdenum delivers Grade 316 superior overall corrosion resistance, especially in chloride conditions where it provides increased resistance to pitting and crevice corrosion. Figure 3.2 shows type of metal powder use for this study (S 316 L-A11). The low carbon form of 316, grade 316L, is resistant to sensitization, or the precipitation of grain boundary carbide. As a result, it is often utilized in heavy gauge (above about 6mm) welded components. Typically, there is not much of a cost distinction between 316 and 316L stainless steel. These grades have exceptional toughness, even at cryogenic temperatures, thanks to the austenitic structure. 316L stainless steel has better creep, stress to rupture, and tensile strength at higher temperatures than chromium-nickel austenitic stainless steels.

Figure 2.14   Material use for this study (S 316 L powder)

The analysis of 316L is identical to 304, however it contains more molybdenum makes it more corrosion resistant compared to 304. For applications that demand high strength and high corrosion resistant, 316L delivers extraordinary functions. Table 2 shows the mechanical properties of S 316 L.

Table 2 Mechanical Properties of S 316 L

Mechanical Properties of S 316 L	
Yield Strength	170 MPa
Tensile Strength	485 MPa
Elongation	40 %

2.11.3 Argon Gas and Nitrogen Gas

Typically, L-PBF machines are set up with argon and nitrogen gas as the process atmosphere. While nitrogen is a diatomic molecule found in the air, argon is a noble gas with its entire outer shell of electrons. The nitrogen molecule is comparatively inert and lacks free electrons, just like argon. However, it can disintegrate and dissolve in the

atomic state of the metal. The nitrogen atoms can then interact with alloying elements and other elements like oxygen, hydrogen, or sulfur (Pauzon, 2019).

316 L pieces achieve high density and raise the overall construction pace by using high laser scanning speeds (Sun et al.,2016). The fatigue properties of 316 L material made by L-PBF are comparable to those of material made traditionally (Riemer et al.,2014). Seldom are the significance of the process gas and the associated process parameters discussed. As a result, only inert argon and nitrogen may be utilized as process gases for SLM. Nitrogen is a molecule that can dissociate, whereas argon is a noble gas. Atoms of nitrogen can then react with oxygen, hydrogen, and sulfur, among other species. In addition to dissolving in the molten metal, they can also combine to generate nitrides with active metals like vanadium, titanium, chromium, etc. The process gas's primary function is to prevent oxidation. The temperature of the powder bed rises dramatically when it interacts with the laser beam, increasing the possibility of stable oxide production. The process chamber volume is flushed with the chosen gas to determine the necessary atmospheric purity, which protects the material from oxidation. After that, the flushed gas is released. Although they are not necessarily reduced to the thermodynamically necessary level, the oxygen and contaminants that were initially present in the chamber are diluted. This keeps happening until the device senses a lower oxygen level and begins to circulate the gas. Machine manufacturers do offer options, usually involving a lot of flushing, to achieve the necessary process environment composition and cleanliness. An alternative approach is to backflush with inert gas after emptying the chamber completely and generating a low vacuum (Renishaw, n.d.). To create the necessary environment before the procedure begins, this may be done multiple

44

times. By removing process byproducts, the guided gas flow also helps to prevent further interaction between the byproducts and the laser beam.

2.12   Parameter Selection

Parameter selection is a very crucial part as a badly selected set of parameters can lead to keyhole formations, balling phenomenon, and insufficient powder fusion. Figure 3.3 provides an example of how the process outcome is affected by the selection of laser power and scanning speed. Lacks-of-fusion porosity arise from insufficient powder melting caused by high laser speed and low laser power. Conversely, selecting an excessively high power level for a certain speed leads to overheating, which in turn causes deeper laser penetration and the production of keyholes—pore structures made of inert gas. The microstructures of layers that have already cemented will be impacted by the deeper penetration brought on by the overuse of laser power. Figure 3.3 indicates that within the safe operating window for minimum flaws, we can raise both the power and speed. Beyond a certain point, however, increasing the power and speed will also cause an unstable melt pool behavior and the balling phenomena, which forms tiny spherical balls and results in discontinuous melt tracks. Finding the ideal window for process parameters is therefore crucial before manufacturing.
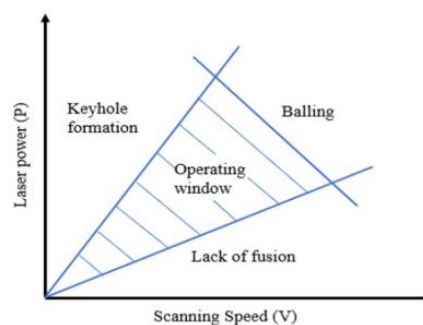

Figure 2.15   Influence of laser power and scanning velocity on the build outcome

45

Nevertheless, because there are so many parameters that are thought to have an impact on the deposition process, it is very difficult to comprehend and optimize every parameter (C. Kamath et al., 2014). Several research have determined that important factors influencing the final part's attributes are laser power, scanning speed, hatching spacing, layer thickness, and scanning techniques.

Table 3 Parameter of Ermaksan Enavision 120 SLM 3D Printer

Name Powder	S316L-0.04
Slicing	
Part Slice Thickness	0.0400 mm
Scan Support every	1 layer
Rescaling	
Scale Center	Platform Origin
Scale X	1
Scale Y	1
Scale Z	1
Chess Pattern Parameters	
Hatch Distance	0.1000 mm
Size X	5.0000 mm
Size Y	5.0000 mm
Field Offset	0.0100 mm
Hatch Sorting	Optimized Sorting
Rotation Start Angle	67.deg
Rotation Increment	67. deg
Shift Factor	4
Filling Orientation	0/90 deg
Field Output Order	Field-Based
Scanning	
Border	
Laser Diameter	0.0750 mm
Laser Speed	900.0000 mm/s
Laser Power	130.0000 W
Following Border	
Laser Diameter	0.0750 mm
Laser Speed	900.0000 mm/s
Laser Power	130.0000 W

Hatches	
Laser Diameter	0.0750 mm
Laser Speed	1000.0000 mm/s
Laser Power	240.000 W
Supports	
Hatches	
Laser Diameter	0.0750 mm
Laser Speed	1000.0000mm/s
Laser Power	240.0000 W
Non-Solid Supports	
Laser Diameter	0.0750 mm
Laser Speed	1000.0000 mm/s
Laser Power	240.000 W

2.13   Specimen Preparation

Specimen prepation of Charpy impact test is conducted by SLM process using Ermaksan Enavision 120 SLM 3D Printer (as shown in Figure 3.4). A set of specimen drawing with dimension refers to ASTM E23 is prepared by using CAD software. The CAD file is then converted into STL file to enable the 3D printer able to print the specimen required. The printing process begins to print the product or specimen layer by layer after the 3D printer software get the STL file. Figure 3.5 shows the flowchart for specimen preparation process and Table 4 shows the procedure to setup the Ermaksan Enavision 120 SLM 3D printer.

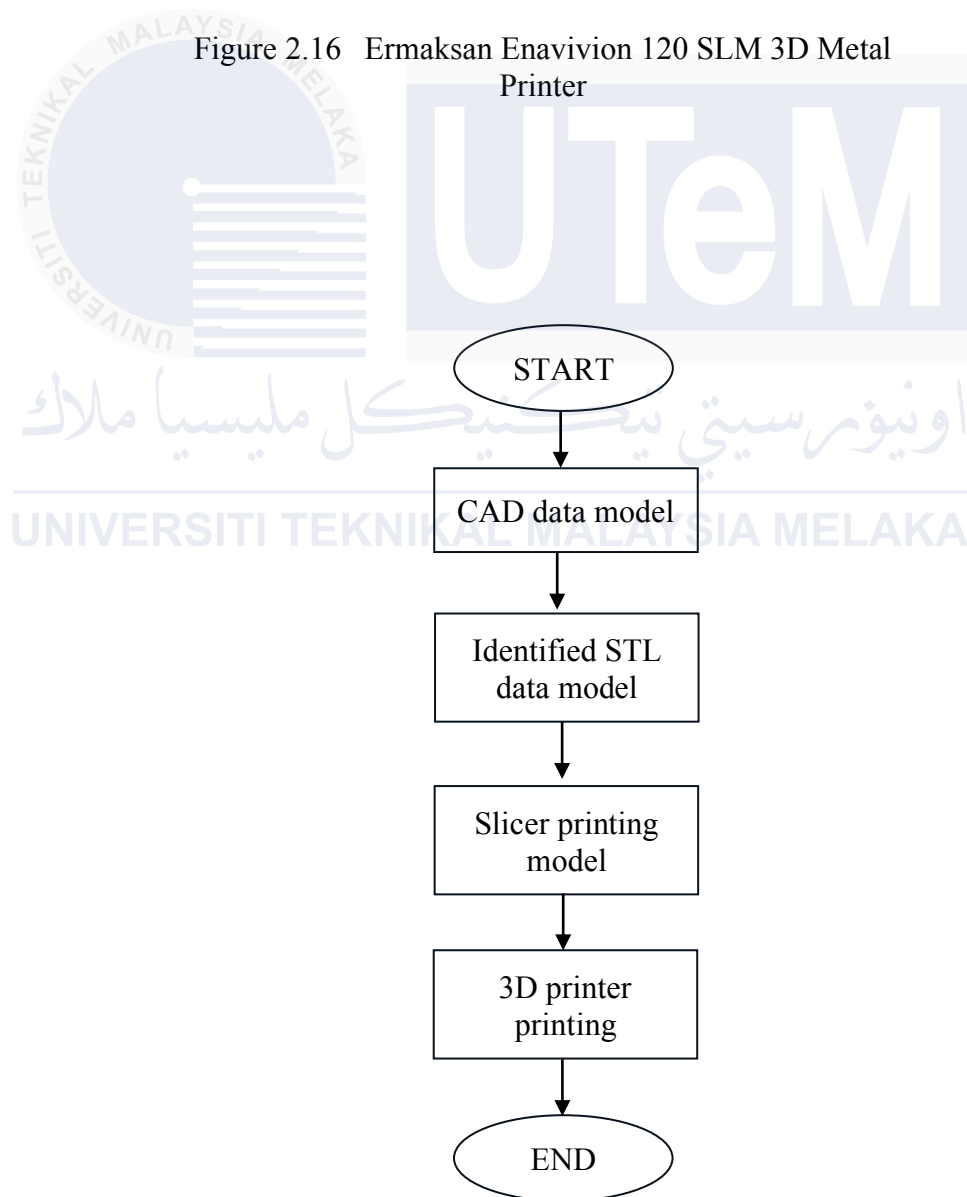Figure 2.16   Ermaksan Enavivion 120 SLM 3D Metal Printer

Figure 2.17   Charpy Impact specimen preparation process

Table 4 Procedure to setup SLM 3D printer for specimen preparation

|	
1.	Check the cables and hoses.
2.	Check the electrical and gas conections.
3.	Switch-on the machine.
4.	Open the gas 6-6,5 Bars.
5.	Wait until the "TwinCat" window goes down.
6.	Wait until the "TwinCat" icon turns the green on the Windows taskbar.
7.	Open the MCP on the Windows menu.
8.	Wait until receiving the MCP icon on the Windows taskbar.
9.	Hold on the MCP icon on the Windows taskbar.
10.	Click the "Web Configuration" on the new window.
11.	Click "STOP-SAVE-START" up-right side on the new page.
12.	Double click to "Enavision.exe" shortcut on the desktop.
13.	Activate the "Laser" on" and "Laser Assign".
14.	Check the "Actual Position" (they have to be variable)
15.	Activate the "Axis enable"
16.	Click the "lamp" icon for inside lights.
17.	Check the "Top Pressure" and "Bottom Pressure", they have to be "0".
18.	Activate the "Front Door" to open the front door.
19.	Set the machine and close the front door.
20.	De-activate the "Front Door" for locking the door.
21.	Select the job file.
22.	Check the "powder increment/layer thickness" ratio (has to be bigger than "1.5")
23.	Check the "Production Set. Zero". It has to be "0".
24.	Choose the job file and wait until receive the total layer.
25.	Push the "PLAY" button for starting the inertization.
26.	Wait until receive the lighting "PLAY" and "PAUSE" buttons together.
27.	Push the "PLAY" button to start the production.
28.	After production wait for both pressures decrease to "0".
29.	Close the gas from gas bottle.
30.	After receive the "0" bar activate the "Front Door" to open.
31.	Remove the powder.
32.	Close the door.
33.	Close the Enavision interface.
34.	Click "SAVE-STOP-CLOSE" on the MCP interface.
35.	Hold the MCP icon on the taskbar and click "NEXT".
36.	Wait until disappear the MCP icon.
37.	Close the Windows as a PC.
38.	Switch off the machine from backside after the screen is out of power.
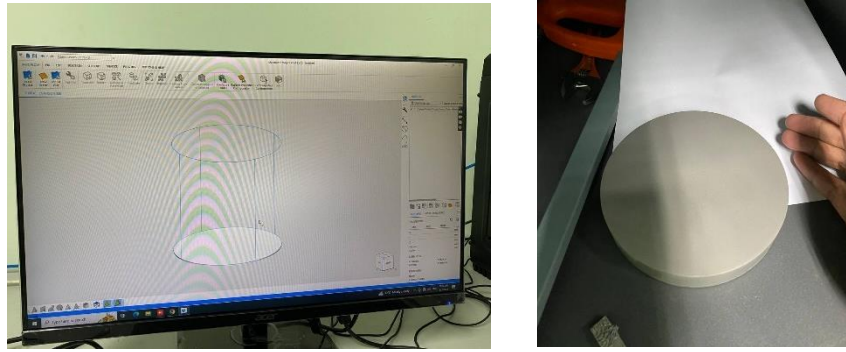
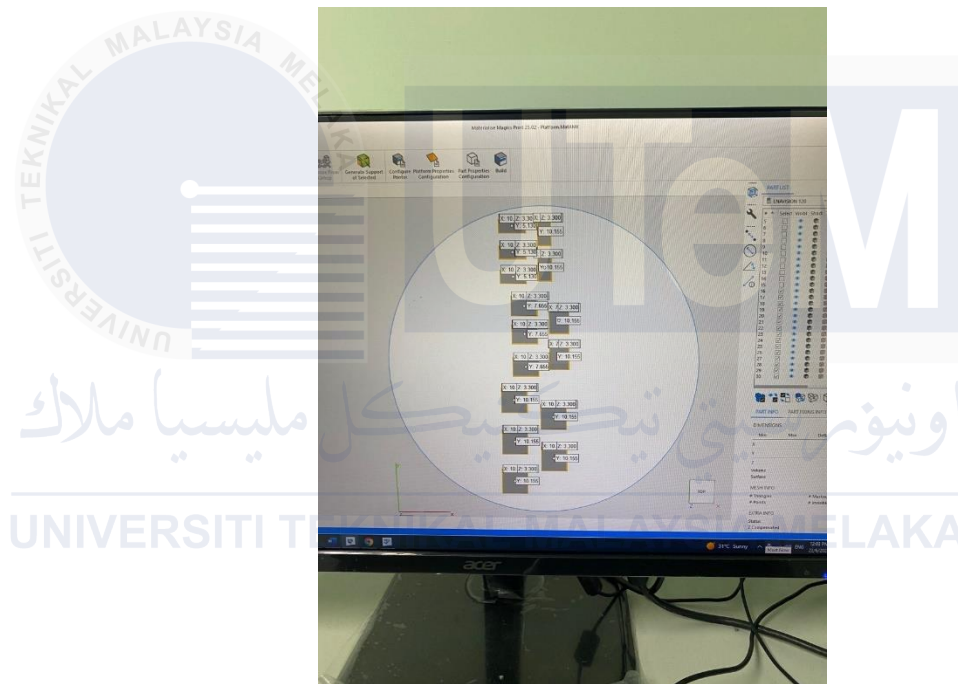Figure 2.18   Base Support of Impact Test Specimen

Figure 2.19   Specimen arrangement of support base

2.14   Experiment Conduct

The specimens for Charpy Impact Test and Tensile Test are determined by cutting the specimen according to precise dimension. Therefore, in this sub-topic, the methodology for each testing to investigate the strength material for three different types of thickness which is 5.0mm, and 7.5mm specimens are shown.

Based in Figure 3.8 is the Charpy Impact Test specimen that has been produced accordingly as refered to ASTM E23, and Figure 3.9 shows specimens that are prepared for running the tensile test which the specimens preparation are refered to ASTM E8.
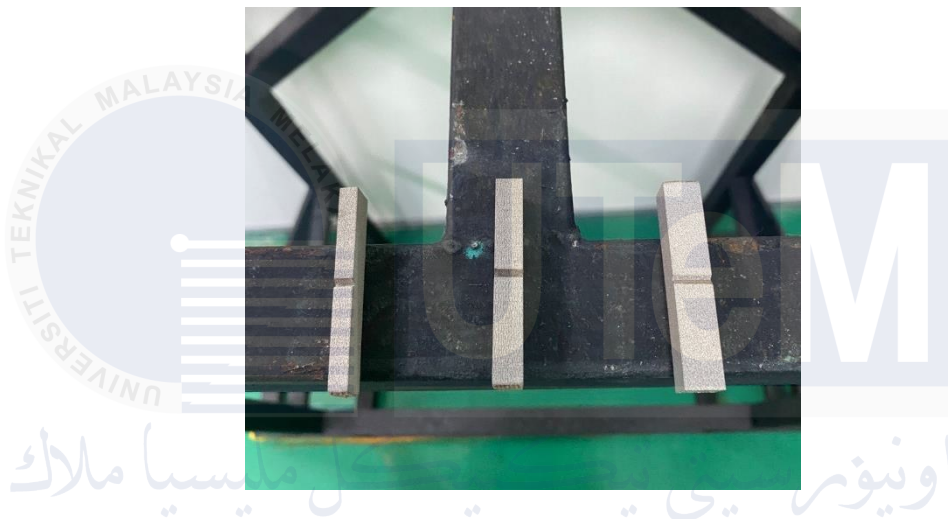
Figure 2.20   Charpy impact specimen

Figure 2.21   Tensile test specimen

Based on the Figure 3.8 and Figure 3.9, the dimension of the Charpy impact specimens are 55mm x 10mm x 10mm, 55mm x 10mm x 7.5mm, and 55mm x 10mm, x 5mm, while for the tensile test, the specimen dimension is 100mm x 10mm x 6mm.

2.14.1 Charpy Impact Test

In this study, a Charpy impact tester Model JBW-500 is used in order to run the Charpy Impact Test as shown in Figure 3.10. The test conducted accordingly to ISO 148-2 and ASTM E23, which are set of standard as refered to the International Organization for Standardization. Prior to conducting the test, the Charpy impact machine is calibrated to guarantee that the results are reliable and accurate.

Figure 2.22   Charpy impact tester Model JBW-500

To ensure that the Charpy machine is in a good operating position, it must be calibrated by releasing the hammer in a spot where no specimen is placed on the anvils.

The machine must read zero on the scale. After the Charpy machine has been calibrated, the portable striker is removed from the hammer in order to insert the strain gauge. After the strain gauge is attached, the striker is repositioned on the Charpy machine's hammer. The Somat eDAQ high acquisition system is then connected to the gauge connection connector, to which the strain gauge is subsequently attached. The computer is connected to the eDAQ system to track the dynamic responses of the strain signal caused by the impact force. Nonetheless, each test item is subjected to the data collection system (Somat eDAQ software) in order to control vibration and provide a smooth signal amplitude.

After configuring the eDAQ software, the Charpy specimen is put on anvils, and the reading scale of absorbed energy is set to zero prior to the hammer being released. Every specimen is put through five distinct tests with varying thicknesses. When the test specimen clogs the machine and it is thoroughly inspected for any damage that could compromise the calibration, the results might be ignored. The quantity of energy absorbed shall not exceed 80% of the actual potential energy, as per refered to ISO-148-2.

2.14.2 Tensile Test

Tensile test is one of mechanical testing which conducted to investigate the material mechanical properties when acting force is applied. This test is also used to study the materil behavior through stress-strain curve along with the ductile-brittle transition. Strain energy and absorbed energy under an axial tension force can be obtained through this testing as well as generate the stress-strain curve also load-displacement graph, respectively. A floor mounted material testing system named Instron Model 5585 Capacity 200 kN is used for the tensile test in this study as illustrated in Figure 3.11.

53

Figure 2.23   Instron Model 5585 Capacity 200 kN

CHAPTER 3

RESULTS AND DISCUSSION

3.1   Introduction

This chapter presents and discusses the effects of the different parameter of the specimens which is the thickness. This chapter analyses the study of Charpy impact test and tensile test between three different types of thickness which are 5mm, 7.5mm and 10mm. It has been highlighted that this chapter explains the study of strength material for additive manufacturing using 3D metal printer which will be resulted into specimen according to ASTM E23 for charpy impact test and ASTM E8 for tensile test.

3.2   Charpy Impact Test Result

Three different thickness of specimens have been tested for the Charpy impact test. The main purpose of conducting the test is to calculate the average value of the impact test data for each specimen of dimension 55mm (L) x 5mm (W) x 5mm (T), 55mm (L) x 5mm (W) x 75mm (T) and 55mm (L) x 5mm (W) x 10mm (T). Table 5, Table 6 and Table 7 shows the tabulated data that have been collected from the analogue scale.

The material's ability to endure unforeseeable loads and absorb energy is gauged by conducting impact test which evaluate its significant characteristic - the impact toughness. The ductility and strength of the tested material are generally considered in

determining the toughness. To perform Charpy test conforming with ISO 148-2 as well as ASTM E23 standards, a highly efficient JBW-500 Computer Pendulum Impact Testing Machine Model is utilized.

Figure 3.1   Charpy impact test specimen

Figure 3.2   JBW-500 Computer Pendulum Impact Testing Machine

3.2.1   Result of 316L Specimen Charpy Impact Test

Table 5 Data result of Charpy impact test for thickness 5mm SS316L specimen
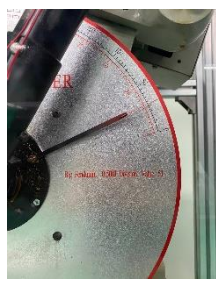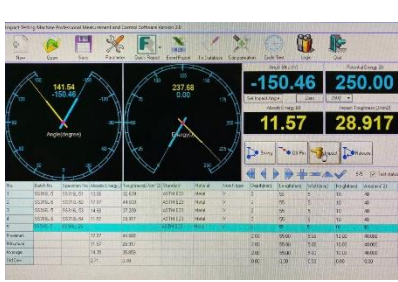
No.	Scale image	WinImpact Display	Value
1			**Energy absorbed** = 13.06 J **Impact toughness** = 32.639 J/cm²
2			**Energy absorbed** = 20.96 J **Impact toughness** = 34.931 J/cm²
3			**Energy absorbed** = 14.88 J **Impact toughness** = 37.209 J/cm²
4			**Energy absorbed** = 11.57 J **Impact toughness** = 28.917 J/cm²
5			**Energy absorbed** = 15.66 J **Impact toughness** = 39.146 J/cm²

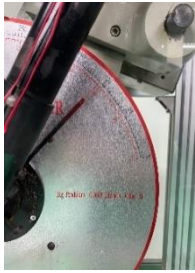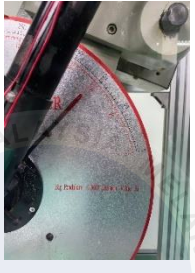Table 6 Data result of Charpy impact test for thickness 7.5mm SS316L specimen
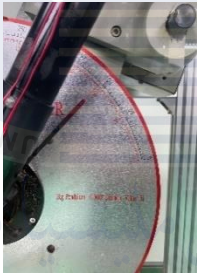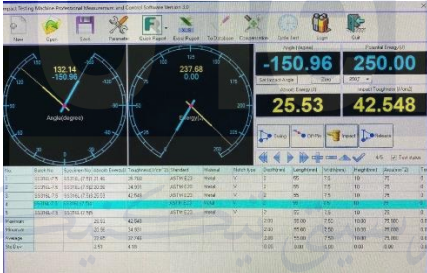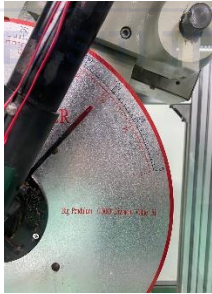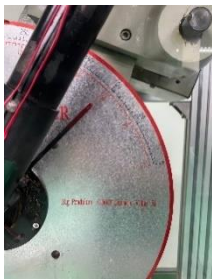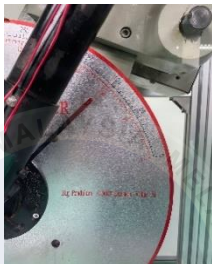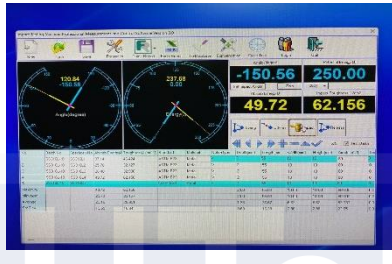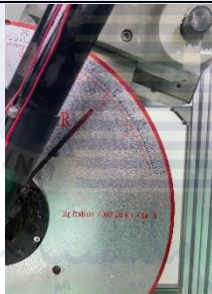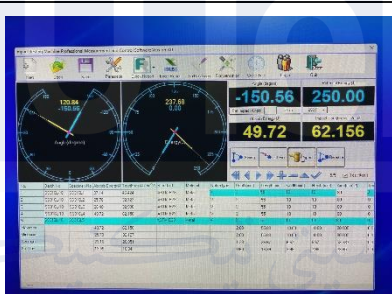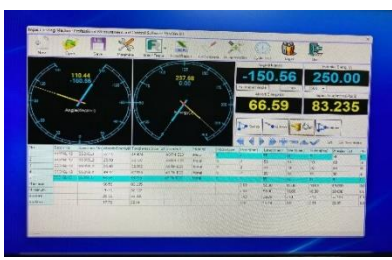
No.	Scale image	WinImpact Display	Value
1			**Energy absorbed** = 21.46 J **Impact toughness** = 35.760 J/cm²
2			**Energy absorbed** = 20.96 J **Impact toughness** = 34.931 J/cm²
3			**Energy absorbed** = 25.53 J **Impact toughness** = 42.548 J/cm²
4			**Energy absorbed** = 17.07 J **Impact toughness** = 28.453 J/cm²
5			**Energy absorbed** = 22.80 J **Impact toughness** = 37.993 J/cm²

Table 7 Data result of Charpy impact test for thickness 10mm SS316L specimen

No.	Scale image	WinImpact Display	Value
1			**Energy absorbed** = 37.14 J **Impact toughness** = 46.424 J/cm²
2			**Energy absorbed** = 25.70 J **Impact toughness** = 32.127 J/cm²
3			**Energy absorbed** = 26.40 J **Impact toughness** = 32.996 J/cm²
4			**Energy absorbed** = 49.72 J **Impact toughness** = 62.156 J/cm²
5			**Energy absorbed** = 66.59 J **Impact toughness** = 83.235 J/cm²

The result of Charpy impact test for thickness 5.0mm, 7.5mm and 10.0mm specimens of S 316 L-A11 specimen shown in Table 5, Table 6 and Table 7. The impact test reading value of 5.0mm thickness for sample 1 is 13.06 J, sample 2 is 20.96 J, sample 3 is 14.88 J, sample 4 is 11.57 J and sample 5 is 15.66 J. The minimum impact test reading value for thickness of 5.0mm is sample 1 which is 13.06 J. It can conclude that the average impact test reading value of the 5 samples for 5.0mm is 15.226 J. As for the impact test reading value of 7.5mm thickness for sample 1 is 21.46 J, sample 2 is 20.96 J, sample 3 is 25.53 J, sample 4 is 17.07 J and sample 5 is 22.80 J. The minimum impact test reading value for thickness of 7.5mm is sample 4 which is 17.07 J. From the 5 samples, it can be concluded that the average impact test reading value for 7.5mm is 21.564 J. Lastly, the impact test reading value of 10.00mm thickness for sample 1 is 37.14J, sample 2 is 25.70 J, sample 3 is 26.40 J, sample 4 is 49.72 J and sample 5 is 66.59 J. The minimum impact test reading value for 10.0mm is sample 2 which is 25.70 J. It can conclude that the average impact test reading value for 10.0mm is 41.11 J.

Table 8 Data of Charpy impact test (absorbed energy) of S 316 L-A11 powder

Specimen thickness	Sample 1	Sample 2	Sample 3	Sample 4	Sample 5	Average
5mm	13.06 J	20.96 J	14.88 J	11.57 J	15.66 J	15.226 J
7.5mm	21.46 J	20.96 J	25.53 J	17.07 J	22.80 J	21.564 J
10mm	37.14 J	25.70 J	26.40 J	49.72 J	66.59 J	41.11 J

Figure 3.3   Specimen after Charpy impact test for 5.0mm

Figure 3.4   Specimen after Charpy impact test for 7.5mm

Figure 3.5   Specimen after Charpy impact test for 10.0mm

Other than that, the Charpy impact test is to investigate the specimen fracture toughness at different type of thickness. The average energy absorbed from the Charpy impact test for specimen thickness of 5.0mm, 7.5mm and 10.0mm were shown in Table 8 and Figure 4.6 shows the specimen of Charpy impact results the specimen thickness of 10.0mm has the highest reading of energy absorbed compared to specimen thickness of 5.0mm and 7.5mm. It can conclude that, the higher the value of energy absorbed, the higher the value of hardness of the specimen. Therefore, specimen with thickness of 10.0mm has the highest energy absorption between 5.0mm and 7.5mm.
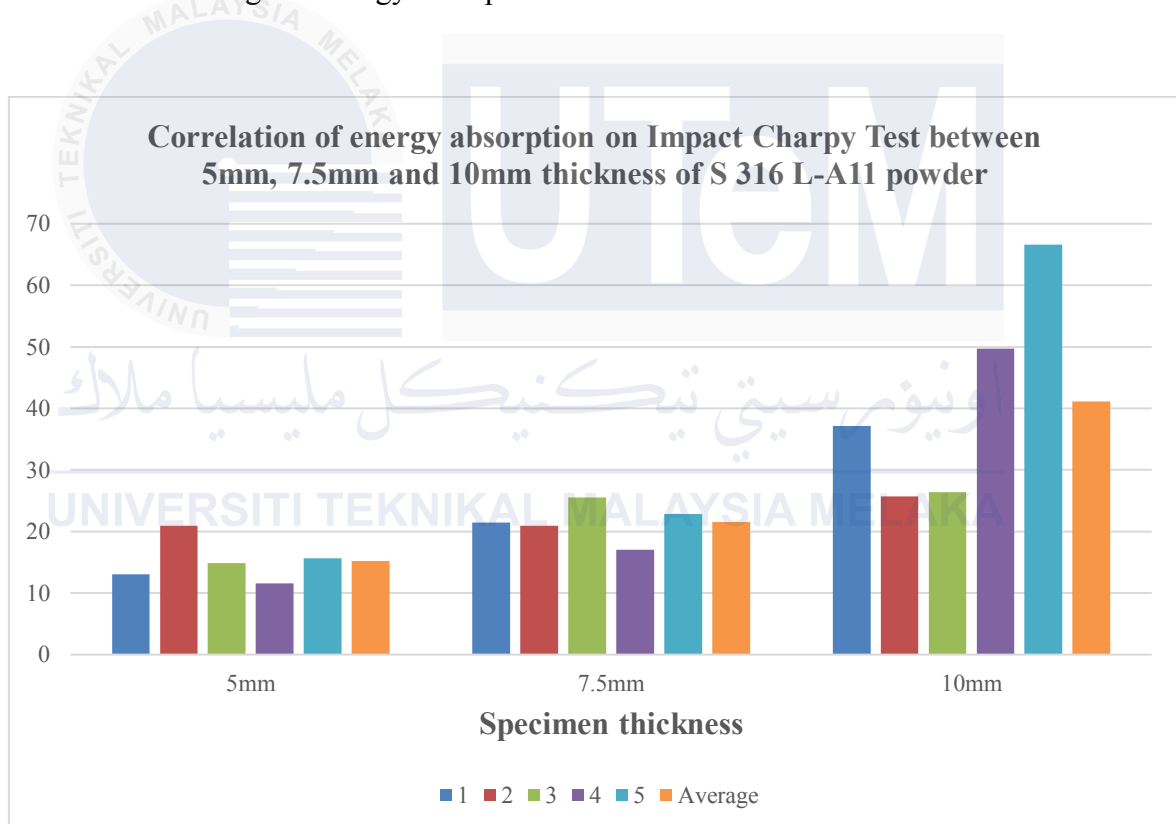

Figure 3.6 Correlation of energy absorption on Impact Charpy test between 5.0mm, 7.5mm and 10.0mm thickness of S 316 L-A11 powder

3.2.2 Energy absorption for Stainless Steel 304

The result of Charpy impact test for thickness 5.0mm, and 10.0mm specimens of Stainless Steel 304 specimen shown in Table 9 The impact test reading value of 5.0mm thickness for sample 1 is 53.75 J, sample 2 is 82.50 J, sample 3 is 57.50 J, sample 4 is 75.00 J and sample 5 is 57.50 J. The minimum impact test reading value for thickness of 5.0mm is sample 1 which is 53.75 J. It can conclude that the average impact test reading value of the 5 samples for 5.0mm is 65.25 J. As for the impact test reading value of 10.0mm thickness for sample 1 is 122.50 J, sample 2 is 130.00 J, sample 3 is 112.50 J, sample 4 is 125.00 J and sample 5 is 111.25 J. The minimum impact test reading value for 10.0mm is sample 5 which is 111.25 J. It can conclude that the average impact test reading value for 10.0mm is 120.25 J.

The Charpy impact test is also used to investigate the specimen fracture toughness at different type of thickness for material Stainless Steel 304. The average energy absorbed from the Charpy impact test for specimen Stainless Steel 304 with thickness of 5.0mm, and 10.0mm were show in Table 9 and Figure 4.7 shows the specimen of Charpy impact results the specimen thickness of 10.0 mm has the highest reading of energy absorbed compared to specimen thickness of 5.0mm. It can conclude that, the higher the value of energy absorbed, the higher the value of hardness of the specimen.

Table 9 Data of Charpy impact test (absorbed energy) of Stainless Steel 304

Specimen thickness	Sample 1	Sample 2	Sample 3	Sample 4	Sample 5	Average
5mm	53.75 J	82.50 J	57.50 J	75.00 J	57.50 J	65.25 J
10mm	122.5 J	130.00 J	112.50 J	125.00 J	111.25 J	120.25 J
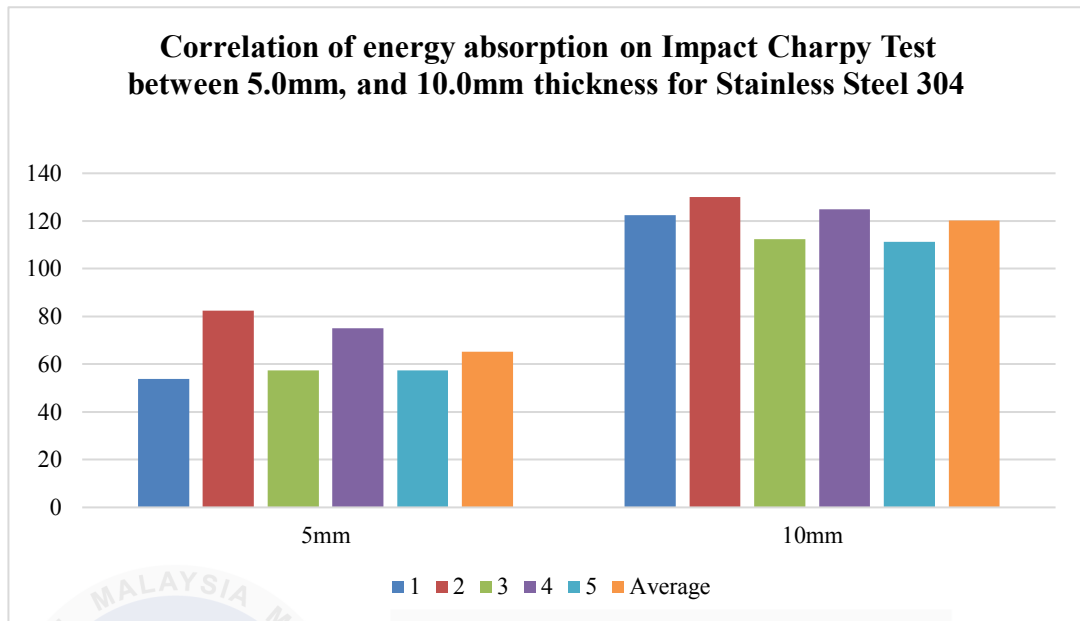
Figure 3.7   Correlation of energy absorption on Impact Charpy Test between 5.0mm, and 10.0mm thickness for Stainless Steel 304

3.2.3   Strain Signal of S 316 L-A11
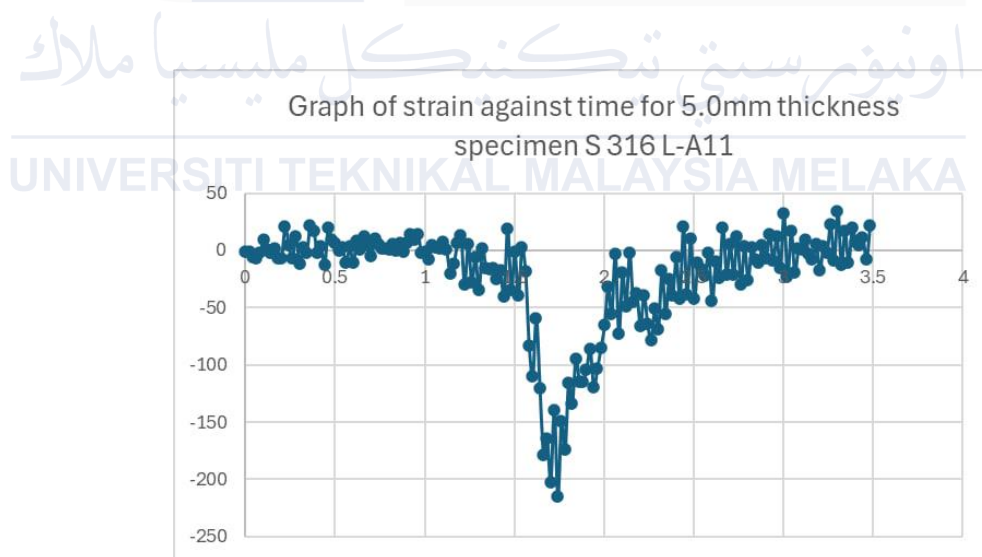
Figure 3.8   Graph of strain against time for 5.0mm thickness specimen S 316 L-A11
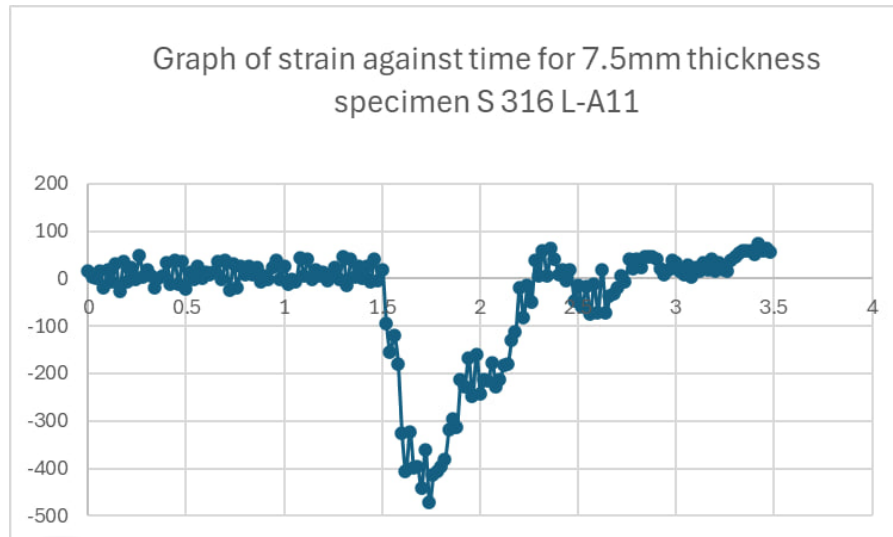
Figure 3.9   Graph of strain against time for 7.5mm thickness specimen S 316 L-A11
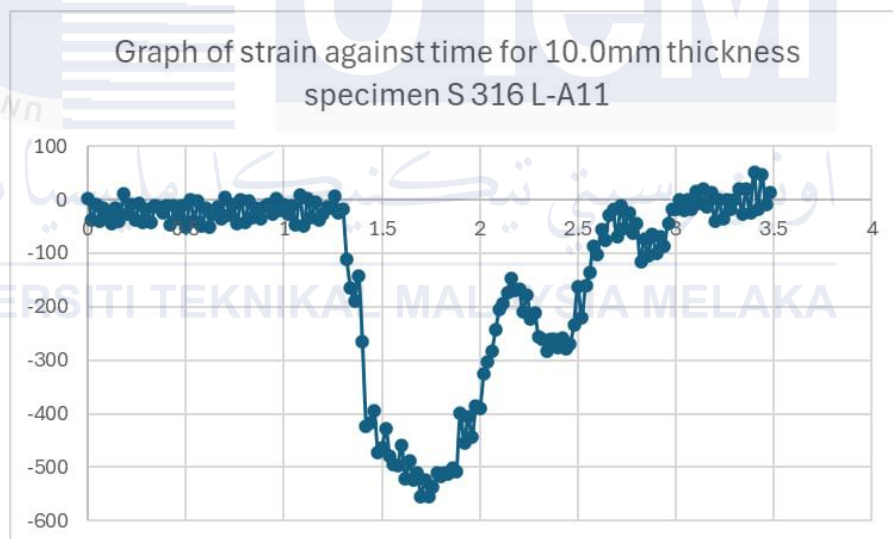
Figure 3.10   Graph of strain against time for 10.0mm thickness specimen S 316 L-A11

65
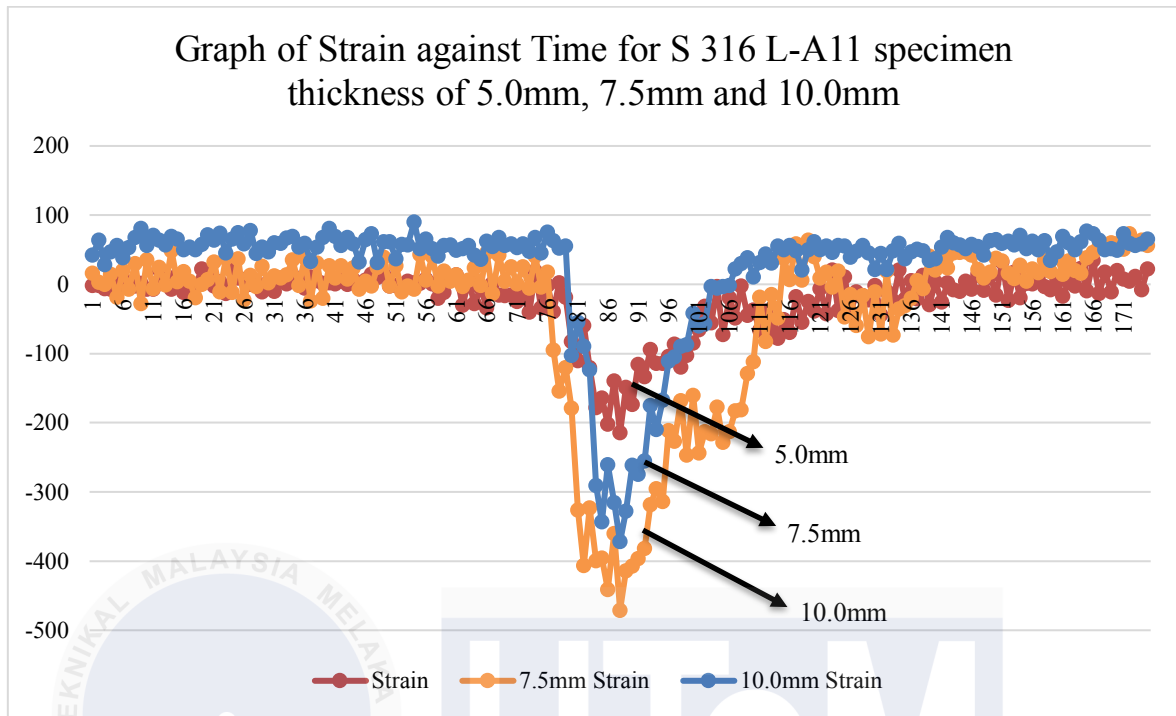
Figure 3.11 Graph of Strain against Time for S 316 L-A11 specimen thickness of 5.0mm, 7.5mm and 10.0mm

3.2.4 Strain Signal of SS 304
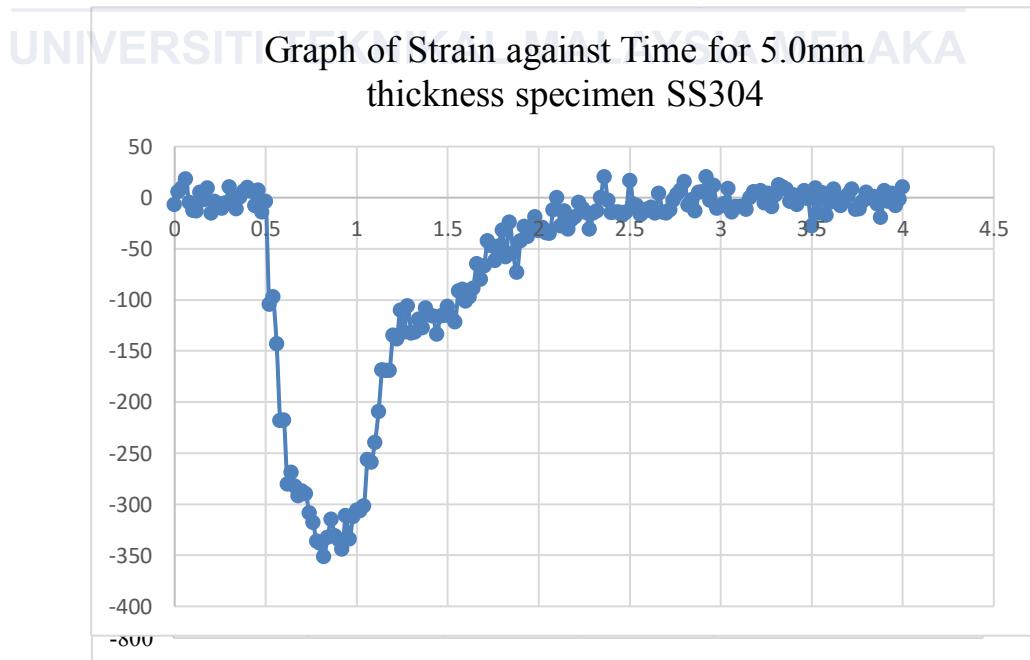
Figure 3.12   Graph of Strain against Time for SS 304 specimen thickness of 5.0mm
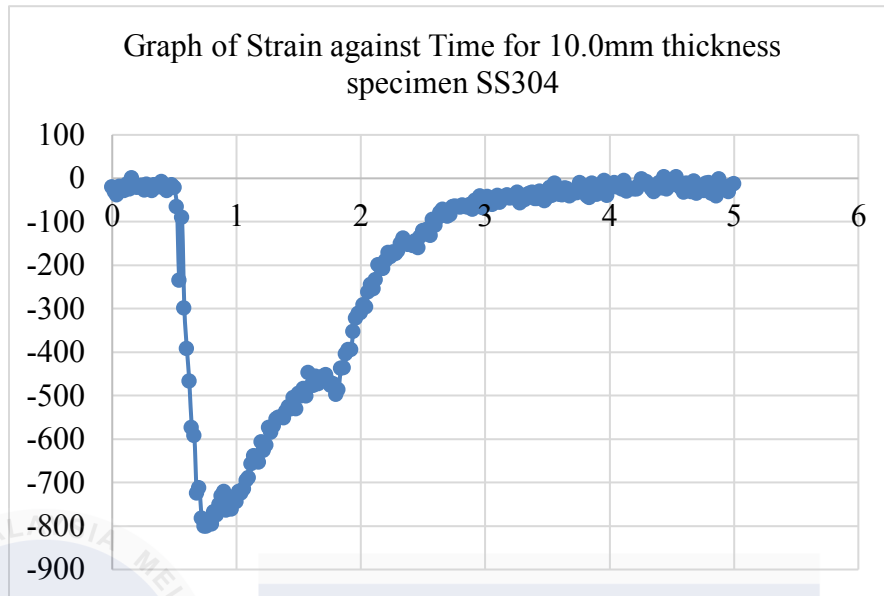
Figure 3.13   Graph of Strain against Time for SS 304 specimen thickness of 10.0mm

3.3   Tensile Test Result

The process of conducting a tensile test is damaging as it uncovers important particulars regarding the metallic material, such as its ductility and strength properties. By gauging how much strain or extension a sample must undergo before rupturing, one can gain insight on the specimen's ultimate tensile strength- which denotes its resistance towards tension-induced fracturing. Consequently, this factor plays an integral role in evaluating the mechanical functionality of any given material. The tensile specimen dimension is 100mm x 10mm x 6mm.

To obtain the required dimensions, the dog bone tensile sample is fabricated and sliced with an EDM wire cutting apparatus. In general, this machine produces a more superior cut trace or surface along with greater precision in terms of diameter cuts.

If a material can resist an external force or stress without undergoing plastic deformation or failure, then it has strength according to mechanical principles. A stress-strain curve reveals the material's characteristics and enable us to precisely identify important parameters such as fracture point, yield limit, and necking threshold. The yield point indicates when elastic behaviour transitions into plastic deformation; beyond this stage lies the onset of deterioration that ultimately culminates in total failure at the fracture point after passing through necking zone.

Figure 3.14   Before and after tensile test for S 316 L-A11

Table 10   The average reading for S 316 L-A11 tensile test

	Maximum Force (kN)	Tensile Strength (MPa)	Maximum Strain (%)	Elastic Force (MPa)	Maximum Displacement (mm)	Break Displacement (mm)
Average	22.701	582.070	23.985	4758.492	9.184	10.786
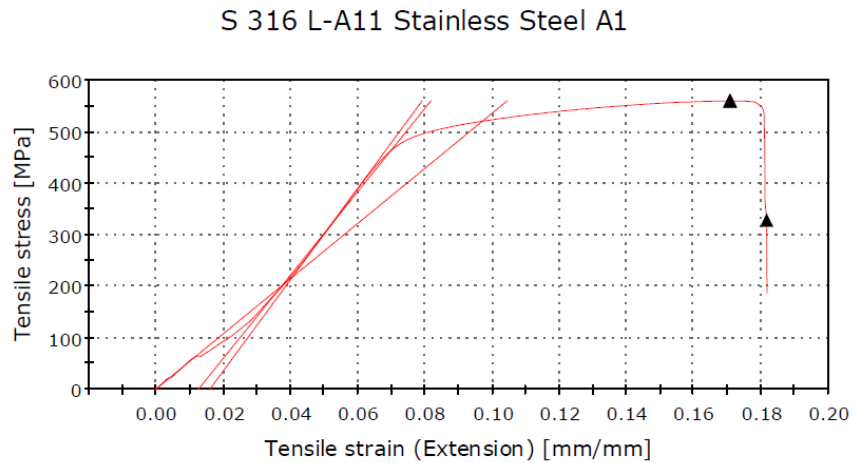
Figure 3.15   Data result of tensile test specimen sample 1 for S 316 L A-11
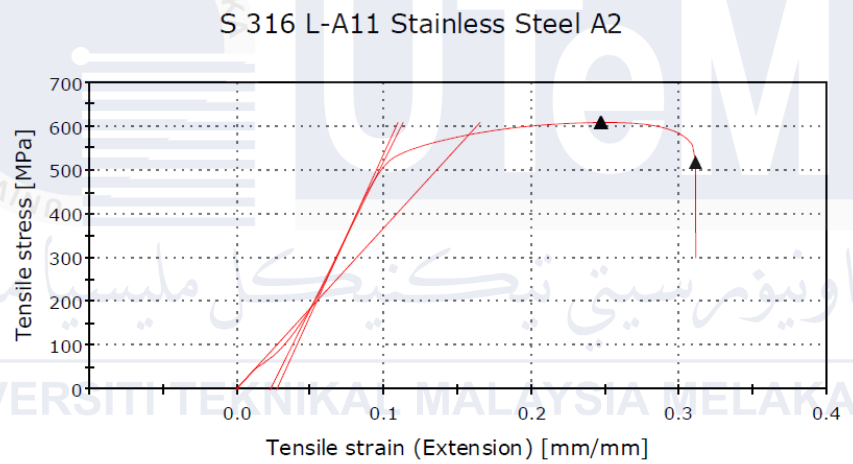
Figure 3.16   Data result of tensile test specimen sample 2 for S 316 L A-11
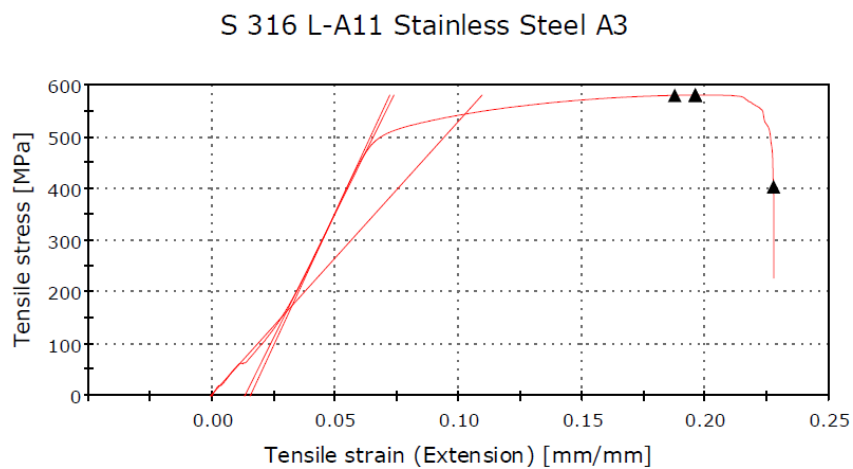
Figure 3.17   Data result of tensile test specimen sample 3 for S 316 L-A11

Based on Figure 4.15, Figure 4.16 and Figure 4.17, it can be concluded that the readings are almost consistent between the 3 specimen samples. Sample 1 takes 21.793 kN to break, sample 2 takes 23.713 kN and lastly, sample 3 takes 22.597 kN to break the specimen. Among those 3 specimen samples, sample 1 has the lowest reading among the 3 samples, while sample 2 has the highest reading among the 3 samples which can be concluded that sample 2 is the strongest sample for S 316 L-A11 with the reading of 23.713 kN.

Furthermore, the result that obtained for Sample 1 to Sample 3 represents that the samples are in optimum reading. Moreover, the maximum strain and strain force for those 3 samples as shown in Figure 4.16 shows that the highest reading is Sample 2 which takes 5332.851 MPa for elastic force. The average reading mechanical properties of S 316 L-A11 are shown in Table 10.

CHAPTER 4

CONCLUSION AND RECOMMENDATIONS

4.1   Conclusion

The results for this study shows that the specimens of S 316 L-A11 of thickness 10.0mm have the capacity to absorb greater impact energy. The specimens that absorbed least amount of energy are specimens of thickness 5.0mm. The area under the strain-time graph, maximum strain, and ebergy absorbed were all significantly influenced by the specimen's thickness. As a result, for the tensile test from maximum strain are directly correlated with specimens' thicknesses.

However, the data from the strain signal of S 316 L-A11 shows that the peak strain values for each specimens thickness are varies among each of the specimens depending on the different thicknesses. According to previous research, there are several factors that might influenced the peak strain values of different specimens. One of the factors is other than specimen thickness is the type of material use. Therefore, in this study for strain signal test result, comparison was made between the peak values of strain signal of S 316 L-A11 and peak values of strain signal of SS 304 in accordance to get more clear vision of the strength of the material. From the comparison results of strain gauge peak values between S 316 L-A11 and SS304, reusults shows that specimen S 316 L-A11 with specimen thickness 5.0mm has the greater value of peak strain signal compared to specimen of SS304. S 316 L-A11 shows that it is the best material for SLM structure and

have bhigher material strength to be implemented for automotive industry compared to S304 material.

On the other hand, the tensile test results in this study shows that the strength material characteristic of S 316 L-A11 that represents by the chemical compositions exists in the material. As the value of the average of tensile test of specimen S 316 L-A11 is 582.070 MPa which is in the range of the tensiles tengh mechanical properties of 316L, therefore it can be said that the material of S 316 L-A11 is suitable to be used as AM material in automotive industry due to its low ductility characteristic which is very useful to be used in automotive manufacturing process for parts designed with hard-to-machine geometries.

4.2   Recommendations

For future improvements, there are several recommendations that need to be highlighted. Assessing mechanical properties, thermal behaviour and microstructural analysis into AM materials to result more comprehensive and accuratable of the material's strength. Next, study on the correlation with printing parameters can be observed to have better understanding of strength material in order to optimize the AM process.

REFERENCES

Sefene, Eyob Messele. (2022). State-of-the-art of selective laser melting process: A comprehensive review. Journal of Manufacturing Systems. 63. 10.1016/j.jmsy.2022.04.002.

Abdullah, R., and Rodzi, A.M., 2011. Labor Utilization and Man to Machine Ratio Study at a Semiconductor Facility. *Journal of Engineering and Technology (JET)*, 2, pp. 75-84.

Rahman, M.N., Abdullah, R., and Kamarudin, N., 2012. Work Study Techniques Evaluation At Back-End Semiconductor Manufacturing. *Proceedings of the 2012 International Conference on Design and Concurrent Engineering,* Melaka, Malaysia, 2, pp. 24-27.

Francois, M. M. et al. Modeling of additive manufacturing processes for metals: Challenges and opportunities. Curr. Opin. Solid State Mater. Sci. 1–9 (2017). doi:10.1016/j.cossms.2016.12.001

Cadazz. CAD software - History of CAD CAM. (2004). Available at: http://www.cadazz.com/cad-software-Sketchpad.htm. (Accessed: 19th December 2023)

Brandt, M. Laser Additive Manufacturing: Materials, Design, Technologies, and Applications. Laser Material Processing (2016)

Dejene, N.D.; Lemu, H.G. Current Status and Challenges of Powder Bed Fusion-Based Metal Additive Manufacturing: Literature Review. Metals 2023, 13, 424. https://doi.org/10.3390/met13020424

Kyu-Tae Kim, Mechanical performance of additively manufactured austenitic 316L stainless steel, Nuclear Engineering and Technology, Volume 54, Issue 1, 2022, Pages 244-254, ISSN 1738-5733, https://doi.org/10.1016/j.net.2021.07.041. (https://www.sciencedirect.com/science/article/pii/S1738573321004642)

Stainless Steel In Automotive Industry (n.d.) Available at: https://www.stanch.com/msg/message-Automotive-Industry-32.htm (Accessed: 19th December 2023)

Materials Science Forum Submitted: 2019-09-06 ISSN: 1662-9752, Vol. 1010, pp 28-33 Revised: 2020-02-18 doi:10.4028/www.scientific.net/MSF.1010.28

V. B. Marco, C. Andrea, Stainless Steels, Politecnico Di Milano, Italy, 2014.

ASM, Materials Selection and Design, in ASM Int. Mater. Park. OH (1997) 2005.

F. Placidi, S. Frashetti, Potential Application of Stainless Steel for Vehicle Crashworthiness Structures, in Proceedings of 1st international conference of super-high strength steels, Rome, Italy, 2005.

K. C. Taylor, Automobile catalytic converters in Studies in Surface Science and Catalysis, Science Direct 30 (1987), 97-116.

Pauzon, Camille & Hryha, Eduard & Forêt, Pierre & Nyborg, Lars. (2019). Effect of argon and nitrogen atmospheres on the properties of stainless steel 316 L parts produced by laser-powder bed fusion. Materials & Design. 179. 107873. 10.1016/j.matdes.2019.107873.

Kruth J. P,Mercelis P., Van Vaerenbergh J.,et al. Binding mechanisms in selective laser sinteringand selective laser melting[J]. Rapid Prototyping Journal,2005,11(1):26-36.

Ng C. C.,Savalani M. and Man H. C. Fabrication of magnesium using selective laser meltingtechnique[J]. Rapid Prototyping Journal, 2011,17(6): 479-490.

Kruth J. P.,Froyen L.,et al. Selective laser melting of iron-based powder.[J] Journal of MaterialsProcessing Technology, 2004,149(1-3):616-622.

Y. Tang, H.T. Loha, Y.S. Wong, et al. Direct laser sintering of a copper-based alloy for creating three-dimensional metal parts[J]. Journal of Materials Processing Technology, 2003, 140:368-372.

Kruth J. P., Leu M. C. and Nakagawa T. Progress in Additive Manufacturing and RapidPrototyping[J]. CIRP Annals - Manufacturing Technology,1998,47(2):525-540.

R.Morrgan, C.J.Sutcliffe, W.O Neill. Density analysis of direct metal laser re-melted 316Lstainless steel cubic primitives[J]. Journal of Materials Science, 2004(39): 1195-1205.

Cacciaguera T.,Osakada K., Shiomi M., et al. The manufacturing of hard tools from metallic powders by selective laser melting[J]. Journal of Materials Processing Technology, 2001, 111(1-3): 210-213.

L. Hao, *et al.* Design and additive manufacturing of cellular lattice structures The International Conference on Advanced Research in Virtual and Rapid Prototyping (VRAP), Taylor & Francis Group, Leiria (2011)

A.A. Zadpoor Mechanical performance of additively manufactured meta-biomaterials Acta Biomater. (2018)

X.Z. Zhang, *et al.* Selective electron beam manufactured Ti-6Al-4V lattice structures for orthopedic implant applications: Current status and outstanding challenges Curr. Opinion Solid State Mater. Sci., 22 (3) (2018), pp. 75-9

S.A. Yavari, *et al.* Relationship between unit cell type and porosity and the fatigue behavior of selective laser melted meta-biomaterials J. Mech. Behav. Biomed. Mater., 43 (2015), pp. 91-100

E. Alabort, D. Barba, R.C. Reed Design of metallic bone by additive manufacturing Scr. Mater., 164 (2019), pp. 110-114

N. Fang, *et al.* Ultrasonic metamaterials with negative modulus Nat. Mater., 5 (6) (2006), p. 452

Z. Hao, *et al.* Lightweight structure of a phase-change thermal controller based on lattice cells manufactured by SLM Chin. J. Aeronaut., 32 (7) (2019), pp. 1727-1732

A. Zargarian, *et al.* On the Fatigue Behavior of Additive Manufactured Lattice Structures Theor. Appl. Fract. Mech., 100 (2019), pp. 225-232

W. Li, *et al.* A novel carbon fiber reinforced lattice truss sandwich cylinder: Fabrication and experiments Compos. A: Appl. Sci. Manuf., 81 (2016), pp. 313-32

C. Yan, *et al.* Advanced lightweight 316L stainless steel cellular lattice structures fabricated via selective laser melting Mater. Des., 55 (2014), pp. 533-541

C. Bonatti, D. Mohr Mechanical performance of additively-manufactured anisotropic and isotropic smooth shell-lattice materials: Simulations & experiments

L. Yuan, S. Ding, C. Wen Additive manufacturing technology for porous metal implant applications and triple minimal surface structures: A review Bioactive Mater., 4 (1) (2019), pp. 56-70

E. Liverani, *et al.* Effect of selective laser melting (SLM) process parameters on microstructure and mechanical properties of 316L austenitic stainless steel J. Mater. Process. Technol., 249 (2017), pp. 255-263

D. Cooper, J. Thornby, N. Blundell, R. Henrys, M. A. Williams, and G. Gibbons, "Design and Manufacture of High Performance Hollow Engine Valves by Additive Layer Manufacturing,"Materials & Design, vol. 69, pp. 44-55, 2015.

S. Biamino, B. Klöden, T. Weißgärber, B. Kieback, and U. Ackelid, "Properties of a TiAl Turbocharger Wheel Produced by Electron Beam Melting," in Fraunhofer Direct Digital Manufacturing Conference, Berlin, Germany, 2014.

M. Cotteleer, M. Neier, and J. Crane, "3D Opportunity in Tooling: Additive Manufacturing Shapes the Future," Deloitte University Press 2014.

A. V. Villalon, "Electron Beam Fabrication of Injection Mold Tooling with Conformal Cooling Channels," M.Sc. Thesis Industrial Engineering North Carolina State University, Raleigh, North Carolina, USA 2005.

Wohlers, Terry T., and Tim Gornet. "History of Additive Manufacturing." Wohlers Report 2014: 3D Printing and Additive Manufacturing State of the Industry Annual Worldwide Progress Report, Wohlers Associates, 2014, pp. 1–34.

Sun, Zhongji, et al. "Selective Laser Melting of Stainless Steel 316L with Low Porosity and High Build Rates." Materials & Design, vol. 104, 2016, pp. 197–204., doi:10.1016/j.matdes.2016.05.035.

Li, Ruidi, et al. "Densification Behavior of Gas and Water Atomized 316L Stainless Steel Powder during Selective Laser Melting." Applied Surface Science, vol. 256, no. 13, 2010, pp. 4350–4356., doi:10.1016/j.apsusc.2010.02.030.

Kruth, J. P., et al. "Part and Material Properties in Selective Laser Melting of Metals." 16th International Symposium on Electromachining (ISEM - XVI) ; Shanghai, China, 19-23 April 2010, Curran, 2014.

Kruth, J. "Selective Laser Melting of Iron-Based Powder." Journal of Materials Processing Technology, 2004, doi:10.1016/s0924-0136(04)00220-1.

Wu, Amanda S., et al. "An Experimental Investigation into Additive Manufacturing-Induced Residual Stresses in 316L Stainless Steel." Metallurgical and Materials Transactions A, vol. 45, no. 13, 2014, pp. 6260–6270., doi:10.1007/s11661-014-2549-x.
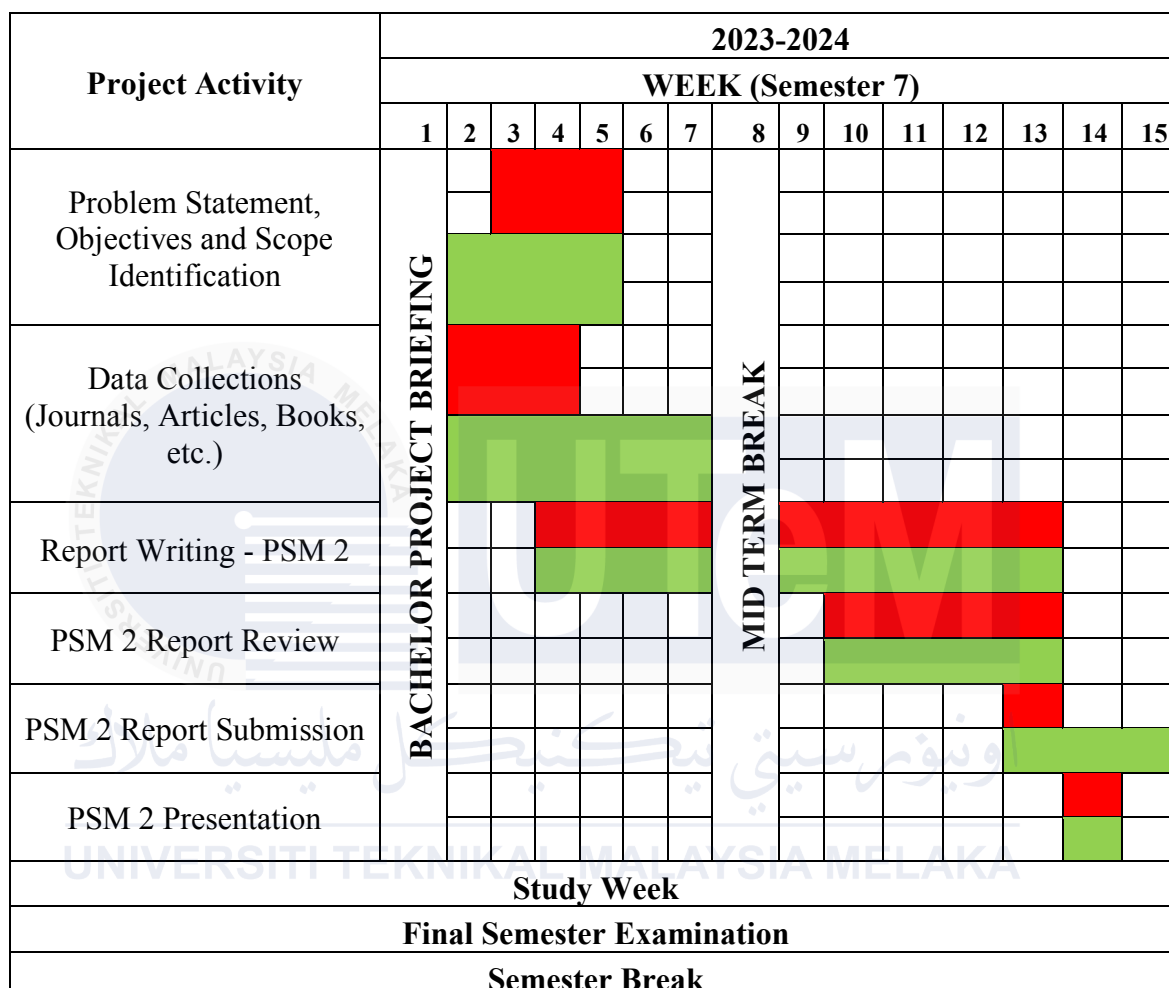
Kamath, Chandrika, et al. "Density of Additively-Manufactured, 316L SS Parts Using Laser Powder-Bed Fusion at Powers Up to 400W." Metallurgical and Mat

Halápi, Dávid & Kovács, Sándor & Bodnár, Zsolt & Palotas, Arpad & Varga, L.. (2018). Tensile analysis of 3D printer filaments. 10.26649/musci.2018.013.

APPENDICES

APPENDIX A   Gantt Chart

Project Activity	2023-2024														
	WEEK (Semester 7)														
	1	2	3	4	5	6	7	8	9	10	11	12	13	14	15
Problem Statement, Objectives and Scope Identification	BACHELOR PROJECT BRIEFING		Plan/Actual					MID TERM BREAK							
Data Collections (Journals, Articles, Books, etc.)			Plan/Actual												
Report Writing - PSM 2				Plan/Actual						Plan/Actual					
PSM 2 Report Review										Plan/Actual					
PSM 2 Report Submission													Plan	Actual	
PSM 2 Presentation														Plan/Actual	
Study Week															
Final Semester Examination															
Semester Break															

■ Plan

■ Actual

80